JOM, Vol. 66, No. 6, 2014
DOI: 10.1007/s11837-014-0978-z

"Bulk" Nanocrystalline Metals: Review of the Current State of the Art and Future Opportunities for Copper and Copper Alloys

M.A. TSCHOPP,[1,2] H.A. MURDOCH,[1] L.J. KECSKES,[1] and K.A. DARLING[1]

1.—U.S. Army Research Laboratory, Aberdeen Proving Ground, Aberdeen, MD 21005, USA.
2.—e-mail: mark.tschopp@gatech.edu

It is a new beginning for innovative fundamental and applied science in nanocrystalline materials. Many of the processing and consolidation challenges that have haunted nanocrystalline materials are now more fully understood, opening the doors for bulk nanocrystalline materials and parts to be produced. While challenges remain, recent advances in experimental, computational, and theoretical capability have allowed for bulk specimens that have heretofore been pursued only on a limited basis. This article discusses the methodology for synthesis and consolidation of bulk nanocrystalline materials using mechanical alloying, the alloy development and synthesis process for stabilizing these materials at elevated temperatures, and the physical and mechanical properties of nanocrystalline materials with a focus throughout on nanocrystalline copper and a nanocrystalline Cu-Ta system, consolidated via equal channel angular extrusion, with properties rivaling that of nanocrystalline pure Ta. Moreover, modeling and simulation approaches as well as experimental results for grain growth, grain boundary processes, and deformation mechanisms in nanocrystalline copper are briefly reviewed and discussed. Integrating experiments and computational materials science for synthesizing bulk nanocrystalline materials can bring about the next generation of ultrahigh strength materials for defense and energy applications.

INTRODUCTION

Mechanical Properties of Nanocrystalline Materials

Nanocrystalline materials result from the grain size of polycrystalline materials being reduced through processing to dimensions on the order of nanometers, which corresponds to drastic increases in the volume fraction (and importance) of grain boundaries and triple junctions within the material. For instance, Fig. 1 shows the evolution of the volume fraction of grain boundaries and triple junctions as a function of grain size, assuming an idealized tetrakaidecahedra grain structure with a grain boundary thickness of 1 nm (solid line). Notice that for grain sizes on the order of 30 nm and smaller, the volume fraction of grain boundaries reaches 10%—approximately an order of magnitude greater than ultrafine grained materials (100 nm to 1000 nm) and several orders of magnitude greater than most coarse-grained polycrystalline materials—which profoundly affects their physical and mechanical behavior.

The interest in nanocrystalline (nc) and ultrafine-grained materials has been motivated by potential improvements in mechanical properties over coarser grained polycrystalline materials[1–5] through the classic Hall–Petch relationship,[6,7] which is defined as

$$\sigma_Y = \sigma_0 + \frac{k}{\sqrt{d}} \quad (1)$$

In this equation, σ_Y is the yield stress, σ_0 is the friction stress required to move individual dislocations, k is a constant, and d is the grain size. The increase in yield strength with decreasing

(Published online May 13, 2014)

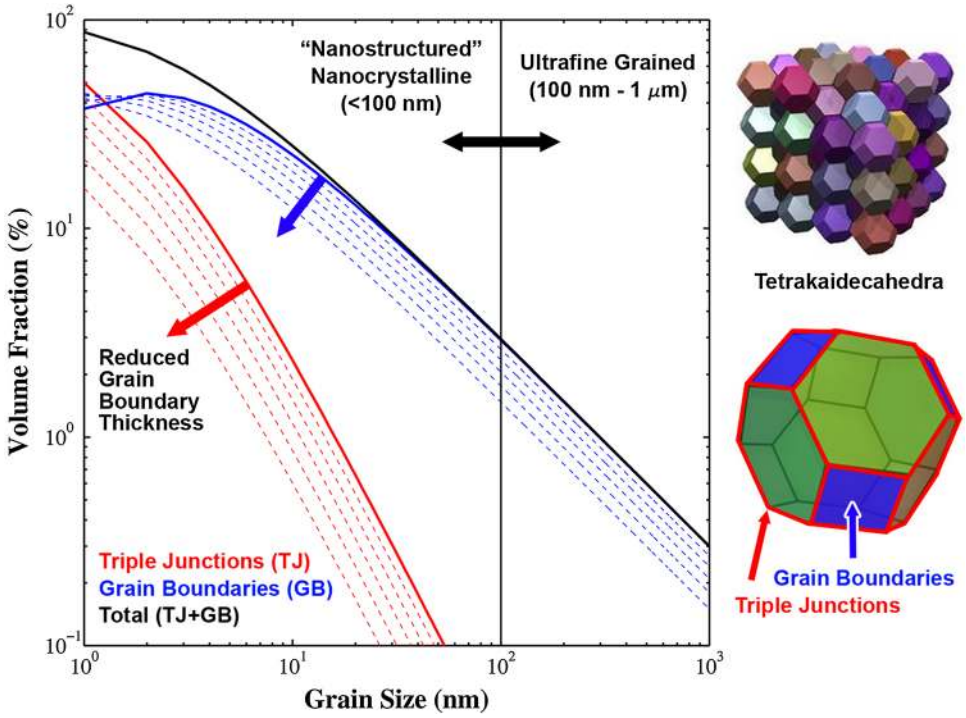

Fig. 1. The increase in the volume fraction of grain boundaries and triple junctions as a function of grain size in the nanocrystalline (< 100 nm) and ultrafine grain (100 nm–1 μm) regimes. These plots are based on space-filling tetrakaidecahedra grains with a grain boundary thickness of 1 nm (thick line), where the dotted lines show the evolution for grain boundary thicknesses of 0.9 nm to 0.5 nm in increments of 0.1 nm.

grain size is attributed directly to the grain boundaries, which serve as obstacles to dislocation motion. Therefore, as the grain size is decreased to the nanoscale, the strength of the polycrystalline materials should increase. Numerous mechanical experiments on nanocrystalline materials have shown that there is a physical limit to the strength increase predicted by the Hall–Petch relation with decreasing grain size,[8,9] i.e., the "inverse" Hall–Petch behavior. Experiments have revealed the breakdown of applicability of the classic Hall–Petch relation at grain sizes typically somewhere between 10 nm and 20 nm, whereby the nc material has a lower yield strength with decreasing grain size in this regime (the mechanisms of which have been proposed by a number of studies[10]). This maximum in the strength of nanocrystalline materials is related to the transition of deformation mechanisms from dislocation-mediated plasticity to grain boundary-mediated plasticity (grain boundary sliding, grain rotation, etc.) as a function of grain size, which has been reported in a number of studies.[11] In general, the amount of strengthening for grain sizes smaller than 50 nm makes nanocrystalline materials an attractive candidate system for future applications over its coarse-grained counterparts. Moreover, the ability to use solute segregation to grain boundaries, the introduction and dispersion of second phases, and the grains of secondary elements/phases can lead to even better mechanical properties.[12]

Defense and Energy Applications

Given the large enhancement in properties related to the fine length scale of nanocrystalline materials, there are a number of potential current and future applications. Some uses of nanocrystalline materials have been found in small components at the micrometer and nanometer scales (e.g., microelectromechanical systems [MEMS] and nanoelectromechanical systems [NEMS] devices, respectively). However, the ability to produce bulk components with nanocrystalline grain sizes can greatly affect the weight and capability of systems-level design. For instance, the increased yield or ultimate strength of nanocrystalline materials may allow for a significant reduction in weight for structural components and parts. While this hypothetical example is naïve in the sense that often structural parts are concerned about more than just yield or ultimate strengths (e.g., fatigue properties, corrosion behavior, ductility, wear, properties at temperature, etc.), this reduction may be used to increase energy efficiency, thereby extending the range of air or land vehicles. Furthermore, a reduction in weight in one part may allow for added functionality in a system (e.g., using the weight reduction to increase sensors, etc.). However, the potential application of nanocrystalline materials depends greatly on our understanding of the properties of nanocrystalline materials and our ability to process these materials without macroscale defects or loss of grain size.

Processing Challenges for Bulk Nanocrystalline Materials

In terms of processing, nanocrystalline materials represent an interesting research area because while their properties relate to the underlying material length scale (grain size), these nanometer-sized microstructures can be produced in bulk materials using various different processing techniques, such as powder metallurgy or deposition approaches. The processing techniques used to produce nanocrystalline materials can be classified in a several ways. The first way of classifying these techniques is based on the microstructure of the starting material used. According to this classification, the processing techniques can be divided into two categories: (I) "bottom-up" and (II) "top-down" approaches. The bottom-up approach starts with atoms, ions, or molecules as building blocks and then these blocks are assembled to form a bulk material (e.g., electrodeposition). Conversely, top-down approaches start with a bulk material and structurally decompose the starting microstructure down to the nanoscale, typically by severe plastic deformation. The second way of classifying these processing techniques is based on the processing technique used to produce the nanocrystalline material. This classification technique contains several different categories: (I) powder metallurgy processing methods, such as mechanical alloying either with external consolidation of ball-milled powders (most typically used) or with in situ consolidation; (II) inert gas condensation and consolidation of nanostructured powders;[13–16] (III) crystallization of amorphous precursors;[17,18] (IV) severe plastic deformation of microcrystalline materials,[2,19,20] e.g., equal-channel angular extrusion (ECAE) or high-pressure torsion; and (V) deposition methods such as electrodeposition,[21,22] physical vapor deposition, or e-beam deposition.[23] All of these processes fall into either the "top-down" (e.g., severe plastic deformation) or "bottom-up" (e.g., electrodeposition and mechanical alloying) approaches.

Much of the difficulty with nanocrystalline materials lies in the production or procurement of "bulk" nanocrystalline materials, however. In general, most top-down methods can readily produce samples in large enough sizes, but the inherent microstructure length scales produced by such processing are often limited to the upper scale of grain refinement, less than 1000 nm but greater than 100 nm (ultrafine grained). The converse is true for the bottom-up approaches. Such bottom-up methods are known to reduce the grain size to the limits of nanocrystallinity (<20 nm). However, the related processing methods struggle either with producing samples with sizes suitability large for proper testing (e.g., electrodeposition or vapor deposition) or with retaining a small grain size during the consolidation to bulk step (powder metallurgy techniques).

In particular, powder processing routes represent a readily scalable process for producing bulk nanocrystalline materials with dimensions much greater than 1 mm. Powder processing techniques are typically a "two-step" processes whereby nanostructured powders are first created and subsequently consolidated at elevated temperatures ($>50\%$ of the melting temperature, T_m). Unfortunately, pure nanocrystalline materials have problems pertaining to thermal stability (grain growth),[24] which often limits the applicable processing techniques as well as any extended applications at moderate to high (and sometimes low) temperatures. This has led to a number of studies that have discussed the inherent problems of nanocrystalline material consolidation, including porosity, insufficient bonding, and impurities (e.g., Refs. 25–27). However, to overcome the thermal stability, several schools of thought have arisen to mitigate grain growth in nanocrystalline materials, thereby permitting consolidation of bulk components/parts while retaining the high mechanical properties.

This article will discuss the methodology, analysis tools and techniques, mechanical and physical properties, and research supporting powder metallurgy processing approaches for producing consolidated bulk nanocrystalline metals. In particular, the objective of this work is to highlight some of the recent progress in (I) bulk nanocrystalline metal synthesis and consolidation, (II) alloy development and synthesis of nanocrystalline metals, and (III) physical and mechanical properties of nanocrystalline materials. Nanocrystalline copper is chosen as a model materials system for this review, in part because of its poor thermal stability (even at room temperature) and because of the extensive coverage in the literature. Moreover, recent experiments with copper alloys have shown the ability to stabilize the grain size at higher temperatures and consolidate bulk nanocrystalline copper alloys,[28–30] which will be discussed throughout the article as an example copper alloy.

SYNTHESIS AND CONSOLIDATION OF NANOCRYSTALLINE MATERIALS

Mechanical Alloying Process

Mechanical alloying is a solid-state powder processing technique that involves impacting mixtures of powder particles (of different elements/alloys) repeatedly with balls of a harder material in a high-energy ball mill (see schematic in Fig. 2). The repeated impacts cause the powder particles to "cold" weld together via plastic deformation, fracture, and then reweld throughout the duration of the milling. This process leads to material transfer within the powder as well as a refined internal microstructure. Several different attributes are associated with mechanical alloying:[31] the ability to finely disperse

second phase particles, to extend the solid solubility limit, to refine the grain size down to the nanometer range, to synthesize novel crystalline and quasicrystalline phases, to produce amorphous (glassy) phases, to disorder ordered intermetallics, to alloy difficult-to-alloy elements, and to induce chemical reactions at low temperatures. For instance, Fig. 2 is a schematic that shows some of the various starting powders that can be used as well as some of the different microstructure variations that can be obtained. Many different techniques and details are associated with mechanical alloying, including milling at cryogenic temperatures (cryomilling). The interested reader is directed to an excellent review by Suryanarayana.[31]

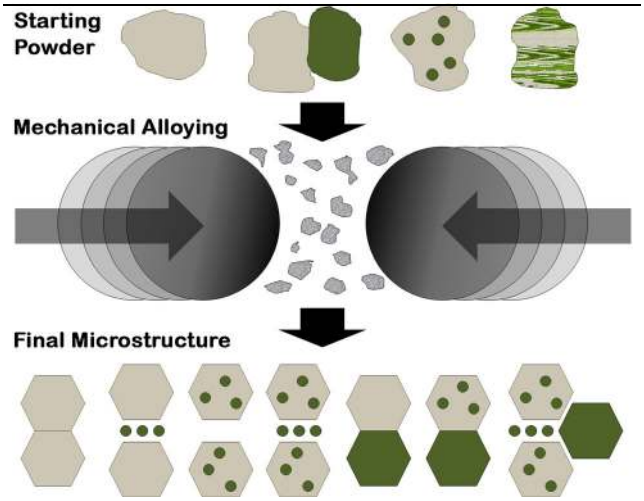

Fig. 2. An example of some of the starting powders and final microstructures attainable with the mechanical alloying process. The starting powder can be of the same element or of different elements, can contain dispersed particles/phases within the powder, or can be a lamellar or layered structure (top, left to right, respectively). The final microstructure can consist of refined grain sizes with/without solute in the grain boundaries, solute in the grains, solid solutions, solute second phases (as grains themselves), or combinations of these.

The process of using mechanical alloying to produce bulk nanocrystalline materials is shown in Fig. 3. There are a number of different types of mills, ranging from laboratory-scale shaker mills (e.g., SPEX 8000 mill, discussed herein) that can produce 10–20 g of powder to commercial-scale mills that can produce thousands of grams of powder at a time. Additionally, these are often classified into low-energy or high-energy mills, depending on the frequency and amplitude of the vibrations of the mill used. The nanocrystalline material flow path starts with loading commercially available powders (in the appropriate proportions, for alloys) and grinding media (typically steel balls) in the right proportion into a vial. This vial is then loaded into a high-energy shaker mill, whereby the back-and-forth shaking motion imparts kinetic energy to the grinding media. The kinetic energy acquired by the balls from the agitation is imparted to the powder particles, thereby subjecting the powder particles to severe mechanical deformation between the balls. With increasing milling time, there is better mixing/dispersion within the elemental/alloy powders and a refinement in the grain size within the powders. After completion of the mechanical alloying stage, the resultant powder often contains a sufficiently small nanocrystalline grain size (< 100 nm). The

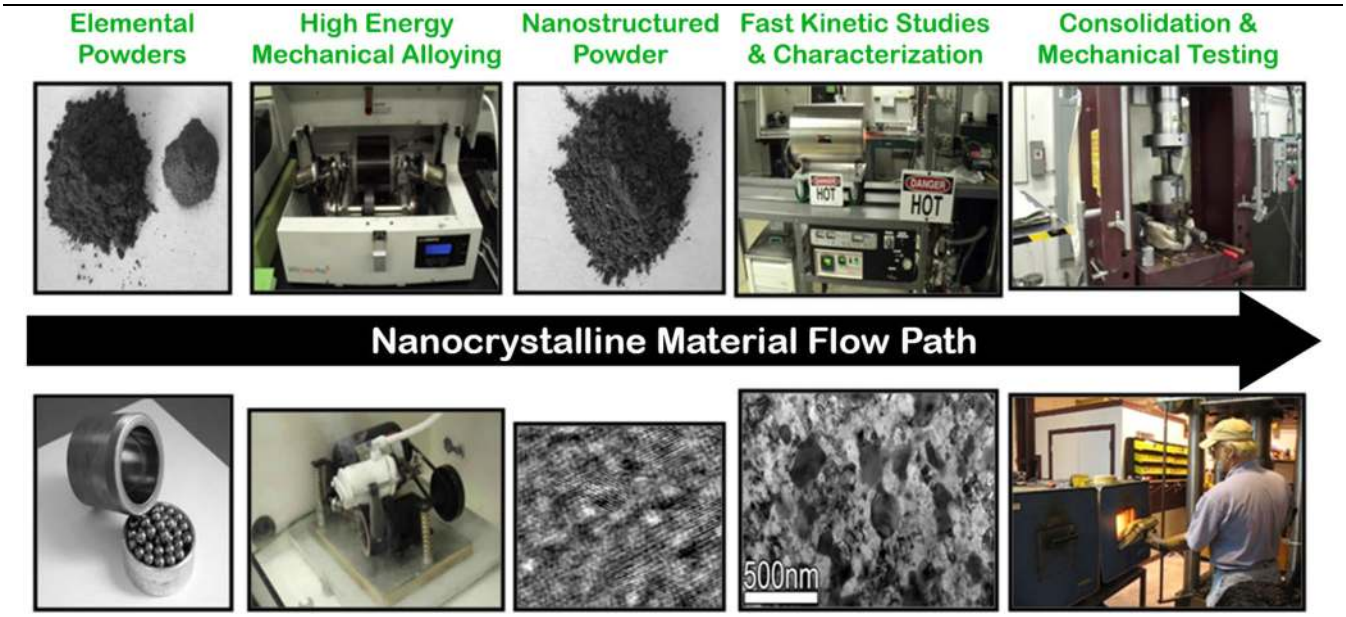

Fig. 3. The nanocrystalline material flow path ranging from (1) the starting elemental powders to (2) mechanical alloying to (3) the nanostructured powder to (4) studies of microstructure and mechanical properties to (5) powder consolidation (numbers denote left-to-right positions of images, respectively).

powder microstructure can be characterized using scanning electron microscopy, transmission electron microscopy, or x-ray diffraction techniques. Subsequent kinetic studies and characterization techniques are often necessary to optimize consolidation processing parameters by understanding the evolution of the microstructure/grain structure with time and temperature. In some cases, second-phase particles or additional phases may manifest in the microstructure at elevated temperatures. Last, consolidation of the nanostructured powder into bulk form uses various powder metallurgy consolidation processes: spark-plasma sintering, equal-channel angular extrusion, flash sintering, hot isostatic pressing, etc. These processes use high pressures, elevated temperatures (typically above 50% T_m), and time to compact and sinter the powders into a fully dense bulk nanostructured part.

Advantages: Grain Refinement Mechanism

The mechanisms for producing nanocrystalline structures through mechanical alloying are based on transmission electron microscopy (TEM) and x-ray diffraction (XRD) studies on powders milled for different times in a high-energy milling process.[32,33] One of the mechanisms is as follows:

1. In the initial stages of ball milling, localized deformation induces shear bands and regions of high dislocation density.
2. After reaching certain strain levels at a particular milling temperature, the dislocation density becomes saturated. Dislocations will start to annihilate and recombine to form small-angle grain boundaries separating the individual grains (subgrains). The sizes of the subgrains formed at this stage are already in the range of 20–30 nm. Further milling of the sample results in the formation of smaller grains in the entire volume of the material.
3. At larger strain levels, the orientations of individual grains become completely random with respect to their neighboring grains. It has been hypothesized that this may be due to the grain boundary-mediated mechanisms, such as grain boundary sliding.

From the above mechanism, it is understood that a large degree of plastic deformation is introduced into the particles during mechanical alloying, which manifests in the microstructure as crystal defects (such as dislocations, vacancies, stacking faults, etc.) and an increased fraction of grain boundaries and triple junctions, as the grain structure is refined. The presence of point, line, and planar defects enhances the diffusivity of solute elements into the matrix; the refined microstructure also decreases the diffusion distances as well as the mean free path between defects. Additionally, the slight rise in temperature during milling further aids diffusion, and consequently, alloying occurs among the constituent elements. The alloying of different elements always depends on the initial particle size and the characteristics of the alloying elements as well as the equipment and process parameters used for the ball-milling process. There are two more possibilities that occur during mechanical alloying:

- **Solid-state amorphization**. Amorphization is believed to occur because the crystalline phase destabilizes from the accumulating structural defects that increase the free energy. The decreasing grain size and the lattice expansion also increase the free energy of the system. Thus, the free energy of the system is increased to a level higher than that of the amorphous phase. Consequently, this results in the spontaneous formation of amorphous structure.[34,35]
- **Extended solid solubility.** The mechanisms for extended solid solubility include the following: (I) the driving force due to the stored energy in grain boundaries,[36] (II) the negative heat of mixing of multicomponent systems due to high oxygen content in the milling process,[37] (III) the fragments with small tip radii are formed during milling-induced deformation such that the capillary pressure forces the atoms at the tips of fragments to dissolve,[38] (IV) the high dislocation density regions act as diffusion paths,[39] and/or (V) the energetic contribution of the phase interfaces enhance the free energy of the composite above that of the solid solution, thus providing the driving force for alloying.[40]

Disadvantage: The Need for Thermal Stability

The most convenient way to deal with consolidation of metal particles is through powder metallurgy techniques such as sintering. Sintering allows for producing useful parts with complex geometries. However, because this method involves the application of heat and pressure, the microstructure of nanocrystalline metals (i.e., the basis for the advanced physical properties) is in jeopardy of coarsening at elevated temperatures. Nanocrystalline copper grows at room temperature in as little as 24 h after deposition/creation[41–44] (this ambient temperature grain growth is observed in other pure metals[41,44]). The rapid grain growth of pure Cu is a function of the low melting temperature (T_m = 1085°C). Under heat treatment to only ~10% of the melting temperature, the grain size of nc Cu doubles.[45] Several studies have reported both strain relaxation and grain growth for pure, nanocrystalline copper between 100°C and 225°C[32–39,45] (~10–20% T_m). Thus, maturing the technology to enable thermal stability in nanocrystalline materials must be realized if steps are to be made toward large-scale applications.

The grain boundaries play a commanding role in the thermal stability of nanocrystalline materials. Conceptually, grain boundaries are only a few

atomic diameters wide and generally account for an insignificant fraction of the microstructure. As the grain size decreases below 10 nm in a nanocrystalline material, the percent microstructure constituted by grain boundaries increases and can be in excess of 50%. Thus, grain boundaries in nanocrystalline materials can account for a large increase of the total free energy of the system. The reduction of this excess free energy, via the removal of grain boundary area, represents a large driving force for grain growth. The driving force/pressure (P) for grain growth, based on the expansion of a curved interface, is:

$$P = A\gamma_b/r \tag{2}$$

where A is a constant, γ_b is the grain boundary free energy per unit area, and r is the radius of curvature of a grain, which is proportional to the grain size. When r is in the range of tens of nanometers, the driving pressure for grain growth is large (approximately hundreds of MPa). It has been demonstrated that pure nanocrystalline metals (Al, Cu, Sn, Pb, Zn, and Mg) exhibit extensive grain growth at room temperature. Metals with higher melting points, such as Co, Ni, and Fe, are not exceptions to this phenomenon and show rapid grain growth over moderate temperature ranges (220–450°C), resulting in grain sizes in the micron range at ~50% of their the respective melting temperatures. Again, this thermal instability limits the overall processing and applications of nanocrystalline metals and alloys. Therefore, it becomes imperative to create alloys that are resistant to grain growth at elevated temperatures.

The thermal stability of these microstructures is essential for adopting nanocrystalline materials in commercial processes and applications. Several investigations on the thermal stability of nanocrystalline materials have been conducted based on controlling the parameters in Eq. 3, the equation for velocity of a grain boundary undergoing curvature driven grain growth, i.e.,

$$v = M \times P = M_0 \exp\left[\frac{-Q_m}{RT}\right] \times \frac{2\gamma_b}{r} \tag{3}$$

where M is the grain boundary mobility, M_0 is the preexponential factor for the mobility term, and Q_m is the activation energy for grain boundary mobility. The pressure P is entirely curvature driven and therefore related to γ_b, the interfacial energy per unit area, and the radius r of the grain.

The stability problem is intrinsic to nanostructured materials. In general, two approaches are used to reduce the velocity of a moving grain boundary (and stabilize the grain structure):[45] by kinetically hindering GB mobility or by thermodynamically lowering the GB energy through solute segregation (i.e., modifying either the kinetic parameter M or the thermodynamic driving force P, respectively).[24,40,46–58] These two approaches are often referred to as the thermodynamic approach and kinetic approach. Because grain boundary mobility follows an Arrhenius behavior, kinetic approaches for reducing grain boundary mobility will eventually be overcome by temperature. Therefore, several researchers have used the thermodynamic approach and have attempted to reduce the interfacial energy, which shows very little temperature dependence. Additionally, the thermodynamic, rather than kinetic, stability could allow for a more rigorous powder consolidation process. Recently, a number of models have been derived that look at these effects independently and the combined effect for systems in which both methods of stability could operate.[46–59]

Powder Consolidation

Many researchers have reported on the enhanced sintering characteristics of nanostructured materials[60,61] that allow high densities to be achieved at much lower temperatures than their coarse-grained counterparts. For instance, Hansen et al.[62] developed a multistage sintering model that relates the normalized densification rate of the specimen ($d\rho/\rho dt$) to the grain size (G), i.e.,

$$-\frac{d\rho}{3\rho dt} = \frac{\gamma}{kT}\left(\frac{\Gamma_V D_V}{G^3} + \frac{\Gamma_b \delta D_b}{G^4}\right) \tag{4}$$

where γ is the surface tension, Ω is the atomic volume, k is Boltzmann's constant, T is the absolute temperature, D_v and D_b are the volume and boundary diffusivities, respectively, Γ_v and Γ_b are density-dependent constants that describe the microstructure, and δ is the grain boundary thickness. As described above, reducing the grain size of the sample can increase the densification rate exponentially. Unfortunately, both grain growth and densification are driven by the same diffusion-based mechanisms. Therefore, the thermal instabilities that lead to an enhanced densification rate also increase the rate of grain growth, resulting in a structure that is no longer nanocrystalline. The decoupling of grain growth and densification is essential for producing bulk specimens that are useful for most engineering applications.[63]

Microstructures that exhibit thermal stability in their grain structure also tend to exhibit a similar stability for their particle structure. The sintering process depends on the reduction of energy from the high-energy state of the finely divided powder to the lower energy of the fully consolidated product. Much of the driving force that leads to densification is based on the overall reduction in surface area. Thermodynamically stable materials are created by reducing the grain boundary and surface energies so that they are essentially the same as that of the bulk material; therefore, the driving force for densification is reduced in the same manner that the driving force for grain growth is inhibited. When

examining Eq. 4, the microstructure and surface energy terms are highly dependent on the interfacial energies associated with the system and directly influence the densification behavior of the material.

Although the thermal stability of these materials tends to inhibit the sinterability of nanostructured materials under conventional conditions, improvements in thermal stability can open a regime of novel consolidation approaches for full densification of nanostructured powders while retaining the nanocrystalline structure. In particular, the application of external pressure during the sintering process, as practiced in hot pressing (HP) and field-assisted sintering technology (FAST) or a combination of pressure and shear, as demonstrated by equal-channel angular extrusion, can greatly improve the tendency for densification.

Pressure-Assisted Sintering

Hot-pressing techniques have demonstrated commercial viability in consolidating metal powders for decades. Hot pressing is typically carried out by heating a uniaxial press during the forming process. The addition of external pressure can cause plastic yielding, which can reduce the sintering temperature and time significantly while achieving the same density in the final product.[64] In the FAST process, a high-pulsed current is passed through the die assembly along with high pressures that results in rapid volumetric heating. This allows for sintering highly dense metals at lower temperatures and much shorter times than traditional sintering processes. The pulsed current induces joule heating at the particle-to-particle contacts, providing true volumetric heating as compared to conventional sintering techniques, which heat from the outside inward. This localized Joule heating reduces the overall driving force required for densification, resulting in full density while retaining the nanocrystalline structure.

Equal-Channel Angular Extrusion

Recent demonstrations of novel processing methods involving temperature, high shear, and high pressure have shown promise for bonding high-strength particulate materials. The ECAE process subjects a billet to a pure state of shear as material flows around an "L"-shaped channel[65–68] (see Fig. 4). ECAE can be performed at elevated temperatures for any number of passes and the billet can be rotated between passes to provide precise texture control for the material.[65–68] This method, which induces severe plastic deformation (SPD) at elevated temperatures, has demonstrated its effectiveness in consolidating metastable powders (e.g., brittle metallic glass powders[69–71]) that have a very narrow processing window and cannot be easily consolidated using conventional methods. In addition, we have shown the utility of ECAE by consolidation to high-density (~99–98%) nanocrystalline

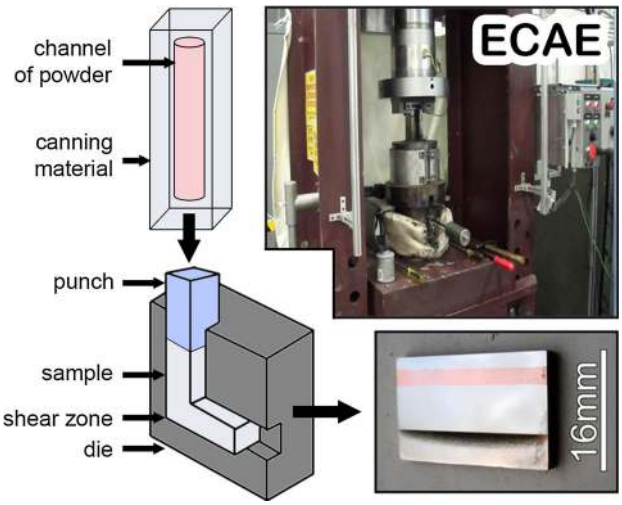

Fig. 4. The equal channel angular extrusion (ECAE) process for consolidation of nanocrystalline powders. The powders are inserted into a canister and heated to an appropriate temperature, and processed using a particular ECAE processing route to fully consolidate the powder material.

Cu-10 at.% Nb, with just a single pass. The addition of high shear can significantly reduce the temperature required to achieve full density and allow the consolidation of metastable microstructures.[72] Another benefit of these SPD methods is that the material samples retain the same basic geometry and cross section as the starting piece, thus allowing for relatively simple scale-up.

ALLOY DEVELOPMENT AND SYNTHESIS OF NANOCRYSTALLINE COPPER AND COPPER ALLOYS

A wide range of studies have investigated the synthesis and properties of pure copper, copper alloys, and copper composite materials using mechanical alloying. In this section, we will briefly discuss several different copper systems that have been investigated using mechanical alloying, their properties (when available), and the potential for using these systems to stabilize the grain structure and improve the mechanical properties of nanocrystalline copper.

Copper Intermetallics and Composites

Several different copper-based systems can potentially improve the stability and mechanical properties of copper. For instance, ordered crystal structures may reduce the overall diffusivity of the material, thereby reducing grain growth. Amorphous phases can be formed using mechanical alloying and subsequent heat treatment can be used to produce a nanocrystalline material. Last, composite materials with a base element (copper, in this case) can be combined with other hard compounds or intermetallics to both improve strength and impede grain growth via kinetic pinning. A further

review of some of these different systems can be found in Suryanarayan[31,73] and the references therein.

Disordered and ordered intermetallic copper-based compounds have been formed using mechanical alloying combined with, in some cases, an additional heat treatment afterward. A number of different copper-based intermetallics have been reported in the literature using mechanical alloying:[31] $CuInS_2$, $CuInSe_2$, $CuInTe_2$, Cu_9Al_4, Cu_3P, $Cu_{2-x}S$, η-Cu_2Sb, $CuSe_2$, Cu_6Sn_5, Cu_3Sn, β-CuZn, γ-CuZn, ε-CuZn, $YBa_2Cu_3O_{7-\delta}$, and Cu_3Ge.[74] While it has been shown that the grain growth kinetics can increase in chemically disordered alloys, the grain growth kinetics can actually be reduced after ordering some intermetallic compounds. This is believed to be caused by the lower diffusivity in ordered structures compared to disordered structures.

Several different amorphous phases have been observed in copper-based systems using mechanical alloying. In some cases, the amorphous phase itself may be desired for its unconventional properties compared to its polycrystalline counterparts. Many different copper-based amorphous phases have been reported in the literature:[31] Cu-30Hf to Cu-70Hf, Cu-42Nb-14Ge, Cu-42Nb-14Si, Cu-35Nb-20Sn, Cu-42Nb-14Sn, Cu-50Nb-5Sn, Cu-11Ni-18P, Cu-20P, Cu-50Sb, Cu-70Sb, Cu-10Sn, Cu-20Sn, Cu-50Ta to Cu-80Ta, Cu-13Ti to Cu-90Ti, Cu-20Ti-20Zr, Cu-50 V, Cu-30 W to Cu-90 W, and Cu-40Zr to Cu-60Zr. Not all of these systems are necessarily 100% amorphous; in some cases, there is a mixture of both an amorphous and a crystalline phase. Also note that for some systems, the predicted range of amorphization is such that another element may actually have a higher atomic percent than the copper (e.g., Cu-Hf, Cu-Ta, Cu-Nb, Cu-Ti, and Cu-W). However, not all systems with Cu as a minor element were listed herein (e.g., some Al-, Cr-, Mg-based, etc.). Interestingly, in these systems, the amorphous phase seems to develop by first forming a fine-grained nanocrystalline phase; as energy is increased in the system, it eventually becomes energetically favorable for the amorphous phase to exist over the large grain boundary energy of the nanocrystalline grain structure. However, upon reheating/annealing, the metastable amorphous phase can transition back to the nanocrystalline grain structure via a nucleation and growth process, yielding small nanocrystalline grain sizes.

Last, to increase strength and to encourage potential grain boundary pinning, the metal matrix can be reinforced with ceramic particles using mechanical alloying, forming a metal-matrix nanocomposite material. The nanostructured composite materials exhibit a higher yield strength and stiffness than the metallic matrix material, while also exhibiting more plasticity than the ceramic phase alone. In terms of particle reinforcement in copper-based nanocomposites, a number of system have been examined:[73] copper with Al_2O_3, B_4C, nanodiamond, Fe_3C, FeS, HfC, MnO, NbC, SiO_2, TaC, and TiC reinforcements. In some cases, even copper with carbon nanotubes are reported to have high strength and good ductility.[75] Of these different (primarily) carbide and oxide reinforcements, alumina (Al_2O_3) and niobium carbide (NbC) are the most common to be combined with the copper matrix. In many cases, increased hardness values (yield strengths) are reported due to a combination of Hall–Petch hardening for the small grain size of the copper matrix and Orowan strengthening for the fine dispersion of oxide/carbides. Consolidation for a number of these systems occurred at elevated temperatures (873 K to 1273 K) and yet retained both grain sizes smaller than 100 nm as well as oxide/carbides with particle sizes smaller than 100 nm. In addition, the volume fraction of ceramic reinforcement, the processing path, conditions, and order of powder additions are also important. For instance, some studies have reported that milling copper with graphite (to disperse the carbon) and *then* adding the niobium powder has resulted in a smaller distribution of NbC particle sizes than combining all powders (in the same fractions) during initial milling.

Addition of Solutes to Stabilize

The more common approach to thermal stability in nanocrystalline materials is to utilize a binary composition whereby the solute will act to either pin the grain boundaries or lower the grain boundary energy (i.e., kinetic and thermodynamic approaches, respectively). Several different solute additions have been explored in an attempt to stabilize the grain size of copper: e.g., Bi,[76] Ag,[77] Fe,[78] Zn,[79] W,[80] Sb,[81] Zr,[82,83] Nb,[84] and Ta.[28,29] In general, the addition of solutes in these systems has shown an improvement in the stability of nanocrystalline copper in terms of moderate to extremely high microstructural stability at elevated temperatures, as shown by Fig. 5. However, the degree of stabilization does not trend with the expected segregation strength—despite a high degree of expected segregation, some alloys do not exhibit significant stabilization (Cu-W[80] and Cu-Bi[85]), while others show good stability despite low expectations of segregation (Cu-Fe[78] and Cu-Ag[77]). In many cases, the thermal stability behavior is linked to the underlying microstructure that forms in these nanocrystalline alloys. Experimental characterization techniques, such as TEM and atom probe tomography (Fig. 6), have helped to understand the fate of solute atoms in these systems, whether it is in the grain boundaries or triple junctions, in a solid solution, in small precipitates or intermetallics, or in larger second phase particles/grains. For instance, in recent studies of a nanocrystalline Cu-Ta alloy,[28,29] TEM images show large Ta grains on the order of >100 nm (Fig. 6, upper middle), TEM images show small (1–2 nm) and medium

(~5–10 nm) Ta precipitates (Fig. 6, upper left), and preliminary atom probe results show a combination of small precipitates and solid solution strengthening by Ta (Fig. 6, far left). This insight into the microstructure helps understand the multiple length scales of microstructure that can affect materials behavior. As the spatial resolution, the element detection range, and the field of view increase for many of these microscopy methods, the effect that solute atoms have on the nanocrystalline microstructure and its thermal stability/mechanical properties can be better understood and can perhaps lead to further engineering of the nanocrystalline structure. Recall that the ability to improve the thermal stability directly affects the ability to consolidate these alloys in bulk form through processes such as ECAE.

Modeling and Simulation Approaches

Material modeling and simulation can help complement experimental observations and measurements while shedding additional insight into atomic-scale mechanisms, providing guidance for alloy design and processing of nanocrystalline materials, and enabling researchers to predict properties and behavior of this class of materials. Modeling and simulation of grain growth in nanocrystalline materials can help us to understand several important aspects of microstructure and processing: the interplay between thermodynamic

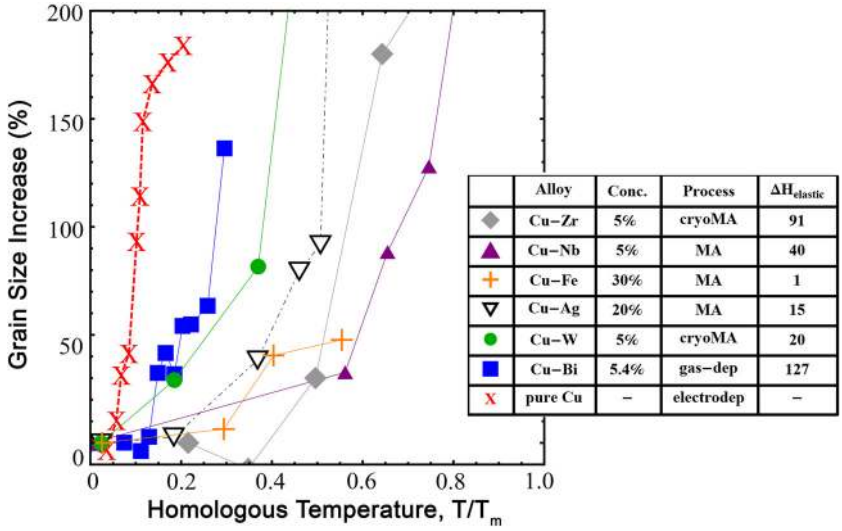

Fig. 5. The increase in grain size (in percent) as a function of the homologous temperature of Cu for several different solutes: Bi, W, Ag, Fe, Nb, Zr (in increasing order of their ability to stabilize the nanocrystalline structure at elevated temperatures). Data taken from references for Cu-Zr,[82] Cu-Fe,[78] Cu-W,[80] Cu-Ag,[77] Cu-Nb,[84] Cu-Bi,[76] Cu-Sb,[81] and pure Cu.[85]

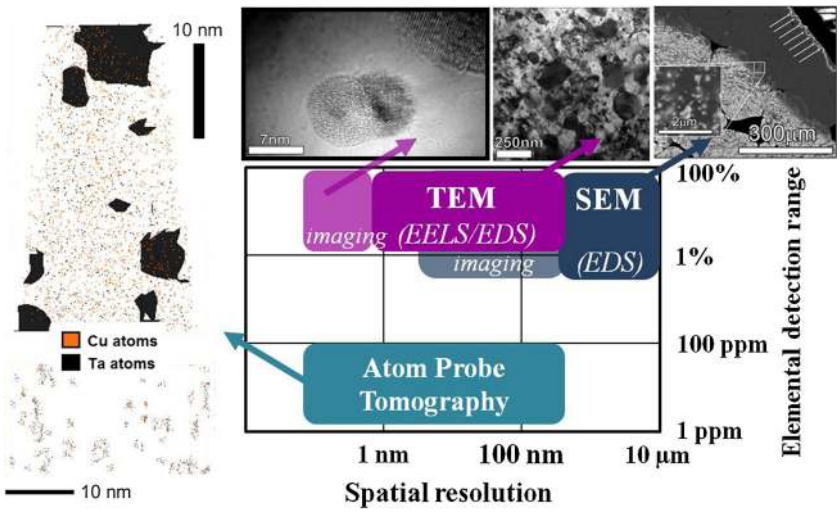

Fig. 6. The spatial resolution and detection range of several material imaging and characterization techniques used to ascertain the final positions of solute atoms within the nanocrystalline microstructure. The inset images show large Ta grains, small and medium Ta precipitates, and Ta in solid solution within the nanocrystalline Cu-Ta system.[28,29]

and kinetic aspects of grain boundaries, the effects of compositional parameters and microstructure on grain growth (e.g., solutes, phases, etc.), the effect of state variables on grain growth (e.g., temperature, pressure), and the changes in grain growth with grain size.

Several recent molecular dynamics simulations have studied the behavior of solute atoms in interfaces and within the grains of nanocrystalline copper. These simulations show that solute atoms randomly positioned (or evolved through Monte Carlo techniques) at grain boundaries in nanocrystalline Cu can retard grain growth[29,82,86,87] and even reduce the grain boundary energy to zero in both general[86–88] and specific[89–91] systems, as is proposed for thermodynamic stability approaches. For instance, molecular dynamics simulations in Fig. 7 show that nanocrystalline Cu rapidly coarsens at 1200 K while the same structure with 5%Ta as Ta clusters (based on TEM images) acts to stabilize the nanocrystalline grain size. While some solutes are effective stabilizers, other solutes are found to have a negligible effect on the grain boundary energy.[89,90] Moreover, simulations show that some solute atoms (dopants) can provide additional strengthening for grain boundary related deformation processes and nanocrystalline materials, in general.[29,92] Furthermore, the development of tools and algorithms that extend both the length and time scales of molecular dynamics[93–95] as well as the ability to characterize and visualize atomistic results[96–100] can aid in using molecular dynamics as a tool for insight into nanocrystalline materials design and behavior. While these simulations can give atomistic details of the nature of these solute atoms in thermal stability and deformation, there have been a limited number of atomistic studies of binary and higher-order alloys compared to the large amount of literature devoted to pure nanocrystalline copper, in part due to the limited number of appropriate interatomic potentials.

Analytical modeling approaches have used thermodynamic parameters (e.g., enthalpy of mixing, elastic enthalpy), state variables (e.g., temperature), solute concentration, grain size, and expressions for grain boundary energy to give guidance for alloying elements that can help mitigate grain growth through the thermodynamic stability approach.[57] These different models use slightly different approaches to the analytical representations of grain boundaries (i.e., a more simplified grain boundary model[57] versus broken bond models and bond interaction energy distributions[50,51,59,101]) but are driven largely by accessible materials properties—the enthalpy of mixing and the elastic or segregation enthalpy of the alloying element. In many cases, these models have been validated against TEM and/or x-ray diffraction data of the stabilized grain size as a function of annealing temperature (e.g., Refs. 57,59) or the success of the system in terms of the characteristic being evaluated (e.g., amorphization). So, while these models often do not contain the atomistic details, they can provide insight and guidance for future nanocrystalline materials design. Several of these articles have brought forward the notion of thermodynamic stability maps to compare

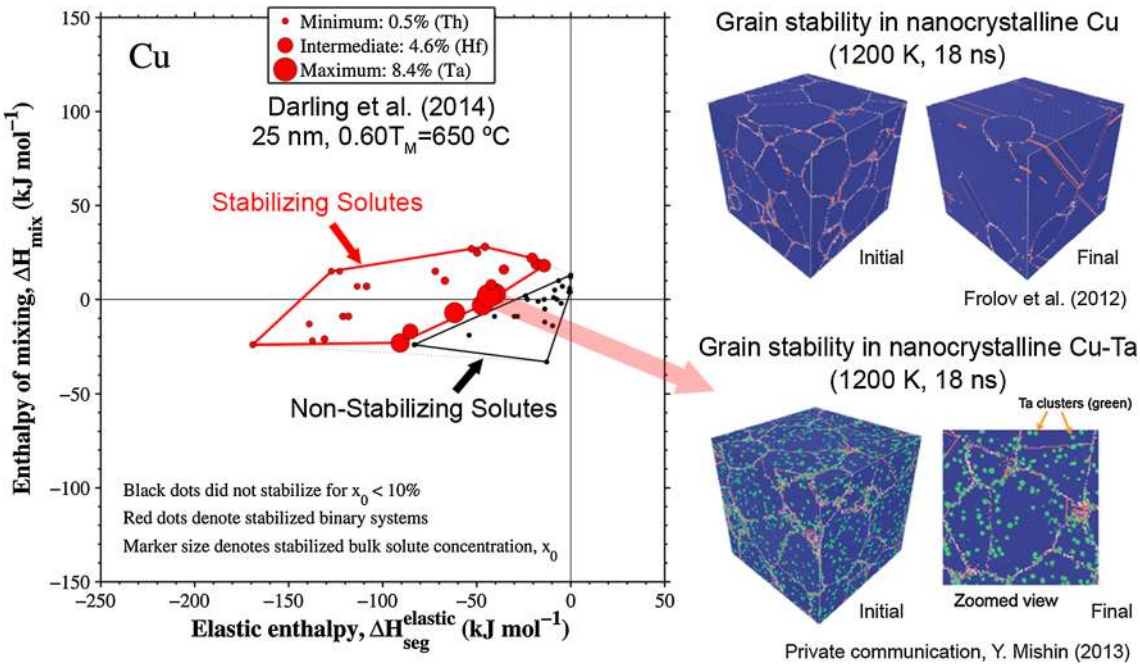

Fig. 7. (left) Thermodynamic stability map for stabilizing nanocrystalline copper at 0.6T_m where the red and black dots indicate the stabilizing and nonstabilizing solutes with respect to the elastic enthalpy and enthalpy of mixing.[57] (right) Molecular dynamics simulations at 1200 K indicate that nanocrystalline Cu rapidly coarsens,[29] while Ta precipitates in the Cu-5%Ta sample stabilize the surrounding nanocrystalline grain size.

with experimental results of thermal stability and to provide guidance for other potential binary systems that could be of interest.[51,57,58] As an example of a thermodynamic stability map, Fig. 7 shows a map for nanocrystalline Cu, in which the red and black dots denote the stabilizing and nonstabilizing solutes, respectively. The outlines of the different systems show that a combination of both elastic enthalpy and enthalpy of mixing contributes to the stabilizing solutes. While a number of solutes are predicted to stabilize the 25-nm grain size at 60% of the homologous temperature, many of these solutes are grain boundary embrittling agents (Bi), are toxic/radioactive (Hg, Cd, Pb, and Ur), have a low melting temperature (Mg), are expensive (Mo, Re, and Hf), or cannot be incorporated into solution through mechanical alloying. In addition to examining the effect on grain boundary energy, the analytical thermodynamic approach can consider the global stability of a segregated nanocrystalline system. As a consequence of the parametric investigations in generating stability maps, nanostructures beyond simple grain boundary segregation, e.g., duplex nanocrystalline or amorphous phases, have emerged as potential stabilized microstructures.[50,51,56] The ability to select solute(s) that contribute to grain boundary segregation stabilization and have a measure of stability with respect to competing phases allows for a wider variety of stabilization and consolidation routes.

Nanocrystalline Cu-Ta Alloys

A recent example of an alloyed binary system in copper that has shown success in thermal stability at high homologous temperatures (>70% T_m) and in bulk consolidation without porosity is the Cu-Ta system.[28–30] The Cu-Ta alloy powders with up to 10% Ta (atomic percent) were synthesized via high-energy cryogenic mechanical alloying and consolidated into bulk nanostructured specimens using ECAE at high temperatures (700°C and 900°C). The subsequent microstructure characterization indicated full consolidation, which resulted in an equiaxed nanocrystalline grain structure for the Cu matrix (~70 nm grain size) along with the formation of Ta precipitates (both small precipitates, ~10 nm, and larger Ta grains, >30 nm), which varied with composition and processing temperature. Remarkably, the microhardness, compression, and shear punch testing indicated, in some cases, almost a threefold increase in mechanical properties above that predicted by Hall–Petch estimates for pure nanocrystalline Cu (see Table I), with good ductility.[30] Further stress relaxation tests substantiated that the strain-hardening behavior and grain size-dependent dislocation activity observed in the nanocrystalline Cu-Ta samples is similar to that in nanocrystalline Ta of a similar grain size. This large increase in strength is attributed to small Ta precipitates/clusters in the Cu-Ta system, which provide a large degree of strengthening above that contributed by Hall–Petch relationship (related to Cu grain size) and Rule of Mixtures hardening (related to larger Ta grains). In fact, the Cu-10%Ta alloy consolidated via ECAE at 700°C has properties similar to nanocrystalline Ta at the same grain size (without 90% of the Ta, though).[30] Interestingly, in the Cu-Ta system, both the thermodynamic stability maps[57] and the molecular dynamics simulations[29] show that Ta is an effective solute for stabilization of the nanocrystalline copper grain structure both through thermodynamic and kinetic mechanisms. The Cu-Ta system has been shown to be a very effective system in terms of thermal stability and strengthening for nanocrystalline Cu with the capability to be consolidated in bulk form using ECAE processing.

PHYSICAL AND MECHANICAL PROPERTIES OF NANOCRYSTALLINE MATERIALS

Nanocrystalline materials present a number of challenges for testing mechanical properties. Small-scale testing techniques are often employed as an effective way of evaluating the mechanical properties of nanocrystalline materials because the quantity of available material often precludes the use of conventional testing dimensions and geometries, which require much larger material volumes. Moreover, relatively easy tests such as hardness can provide insight into the state of the microstructure (e.g., a large decrease in hardness after high-temperature consolidation may signal that the grain size has increased). Several testing techniques can provide information about the mechanical properties of nanocrystalline materials. For example, shear punch testing has re-

Table I. Hardness and quasistatic yield strength of nc Cu-Ta that was consolidated with ECAE at various temperatures[30] compared to nc Cu and nc Ta (in GPa)

		Cu-1%Ta 700°C (168 nm)	Cu-10%Ta 900°C (213 nm)	Cu-10%Ta 700°C (70 nm)	nc Cu[4] (70–250 nm)	nc Ta[102,103] (44–250 nm)
HV		2.12	2.12	3.75	1.35–1.0	4.1–2.5
HV/3		0.7	0.7	1.23	0.45–0.35	1.36–0.83
QS	σ_{YS}	0.7	0.66	1.1	0.45–0.35	1.3–0.9

YS yield strength.

cently been gaining attention as one such technique.[104–106] In addition to minimal sample preparation, the spatial resolution is quite high; therefore, only 1–2 mm^2 of surface area is required for an individual test. In the past few years, this technique has been employed to ascertain deformation mechanisms and characterize material properties of nanocrystalline materials through (I) using various tests, such as stress relaxation tests, and through (II) determining the underlying material properties, such as the activation volume.[107] The physical activation volume is critical for determining the rate-controlling step of the specific plastic deformation mechanism that governs the ductility of nanocrystalline metals; it is related to the strain-rate sensitivity of the material, and it has a definite value and stress dependence for each atomic process.[108] In addition to shear punch testing, there are other testing techniques for evaluating mechanical properties in specimens of various sizes, such as compression, tension, micropillars, and Kolsky bar testing. In fact, for many of these techniques, innovative setups are pushing the lower bound of the specimen sizes.[109,110] Some of the following discussion is based in part on the review of mechanical properties of nanocrystalline materials by Meyers et al.[4]

Mechanical Properties

Elastic Modulus

Nanocrystalline materials are typically produced by SPD. The very nature of such processes lead to microstructures which contain high dislocation densities in addition to the inherently high grain boundary area. As both are structural defects associated with increased free volume, the density of a nanocrystalline material can be lower than that of a well-annealed coarse-grained material (i.e., close to the theoretical density). For instance, it has been reported for nanocrystalline Ni that this discrepancy in density can be as much as 3%, with 80% of discrepancy attributed to the dislocation density and the remaining attributed to grain boundaries.[111] This ratio will change with the average nanocrystalline grain size. The percentage of microstructure occupied by grain boundaries for 3-nm grain size is in excess of 50%; compare this to a 15-nm grain size, which has less than 20% occupied by grain boundaries. The extra free volume associated with grain boundaries[112,113] leads to a reduced elastic modulus as compared to that of a perfect lattice. Reports on the elastic modulus of nanocrystalline copper produced via ECAE state a decrease of 10–15%.[15] Early reports indicating as much as 30–50% reductions are now attributed to processing defects.[114]

Yield Stress and Hardness

The yield stress of a material is known to depend strongly on the grain size through the Hall–Petch relation (Eq. 1). A general rule of thumb is while strength gains are attained by decreasing the grain size from 10 μm to 100 nm, the most dramatic strength gains are only made possible at grain sizes below 50 nm (~10% volume fraction of grain boundaries, Fig. 1); the size of 50 nm is the approximate length scale at which the traditional deformation mechanisms of dislocation-mediated behavior change due to the increased fraction of grain boundaries and triple junctions. For instance, instead of dislocation pileup driving the stress increase, the nucleation of dislocations from the grain boundaries becomes the predominant deformation mechanism driving the increased strength; atomistic modeling has shown that dislocation nucleation is associated with the grain boundary structure, free volume, and stress state at the boundary.[115–118] At the smallest grain sizes, grain boundary sliding, grain rotation, and grain coalescence become the predominant modes of deformation, again shifting the deformation mechanism and, in some cases, contributing to the so-called inverse Hall–Petch behavior. The maximum magnitude of yield strength can approach or exceed an order of magnitude increase over conventional coarse-grained materials[26,119] and is typically reported in materials with grain sizes of <20 nm.

The material hardness generally follows the same trend as the yield strength.[26] However, several examples have been given indicating that at grain sizes <50 nm some materials undergo a softening effect known as the inverse Hall–Petch relationship (e.g., Ref. 120). Several reasons for this effect have been given such as diffusional creep and stress-induced grain growth under the indenter. In addition to softening, a substantial increase (50% or less) in hardness has been reported after annealing some nanocrystalline materials; this has often been attributed to recrystallization of amorphous phases and/or grain boundary relaxation. Figure 8[5,36,120–132] plots a number of mechanical properties (hardness, compression, and tension tests) as a function of the inverse grain size (i.e., Hall–Petch relationship, Eq. 1). Here, the yield stress is plotted on a separate axis and is scaled by a factor of three from the hardness to compare the mechanical properties from all studies. The Hall–Petch hardening is quite evident from the 15 different studies, as expected, but interestingly only Chokshi et al.'s[120] data indicate the inverse Hall–Petch behavior in copper. The remaining data indicate that the strength is somewhat constant at very small grain sizes (<10 nm). In either case, the data indeed indicate that there is a maximum strength that can be obtained in nanocrystalline copper that is on the order of 0.9 GPa.

Ductility

In conventional materials, refinement of the grain size usually leads to ductility enhancements. However, most nanocrystalline materials report a limited amount of ductility as compared to their coarse-grained counterparts (e.g., see papers by Koch[12,25] and Ma[27,129]), which prompted the investigation of

routes to improve the ductility of nanocrystalline materials.[27] The three major sources given for the limited amount of ductility are:[12] structural artifacts from processing, instability in tension, and crack nucleation instabilities. Artifacts from processing that contribute to poor ductility include porosity, insufficient particle bonding, and contamination such as oxides, nitrides, surfactants, and chemicals used in deposition techniques, just to name a few. In many cases, nanostructured materials made via mechanical attrition involve synthesis of particulates that are scaled up with sintering operations to make usable samples for testing. The approach to this sample consolidation technique is to produce samples with complete particle bonding (100% dense). In the past, quite frequently porosity from incomplete densification was still an issue with this technique. However, within the last decade, there are increasingly more examples and strategies for obtaining bulk, fully densified nanocrystalline materials produced via ball milling;[133] subsequent consolidation demonstrates that these materials can possess good ductilities while retaining much of the strength of nanocrystalline materials[119,122,134] (i.e., 14% tensile ductility or potentially higher in Refs. 119, 122).

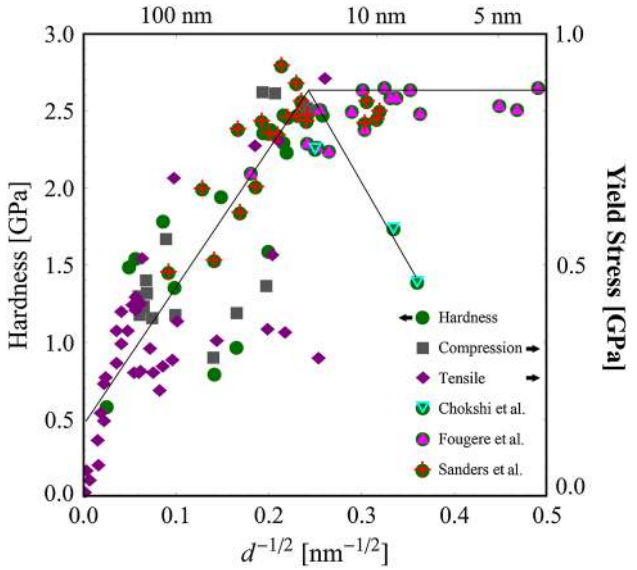

Fig. 8. Hardness and yield strength (compression and tension) as a function of grain size for multiple nanocrystalline copper references from the literature (hardness,[36,120–124] compression,[121,123,125–128] and tension[5,121,122,125,128–132]).

In terms of nanocrystalline copper, the ductility/strength trade-off in nanocrystalline copper is illustrated by plotting the uniform elongation versus the yield strength (Fig. 9). Because reducing the grain size increases the yield strength,[121,135–139] the uniform elongation also decreases (coarse-grained Cu is shown for comparison[140,141]). The solid line shows the general trend between ductility and strength. However, several recent advances in microstructure design and consolidation are pushing the strength and ductility beyond this limit, e.g., bimodal nanocrystalline/coarse-grained Cu,[142] nanotwinned Cu,[143] "artifact-free" nanocrystalline Cu,[144] and cryomilled in situ consolidation of Cu.[134]

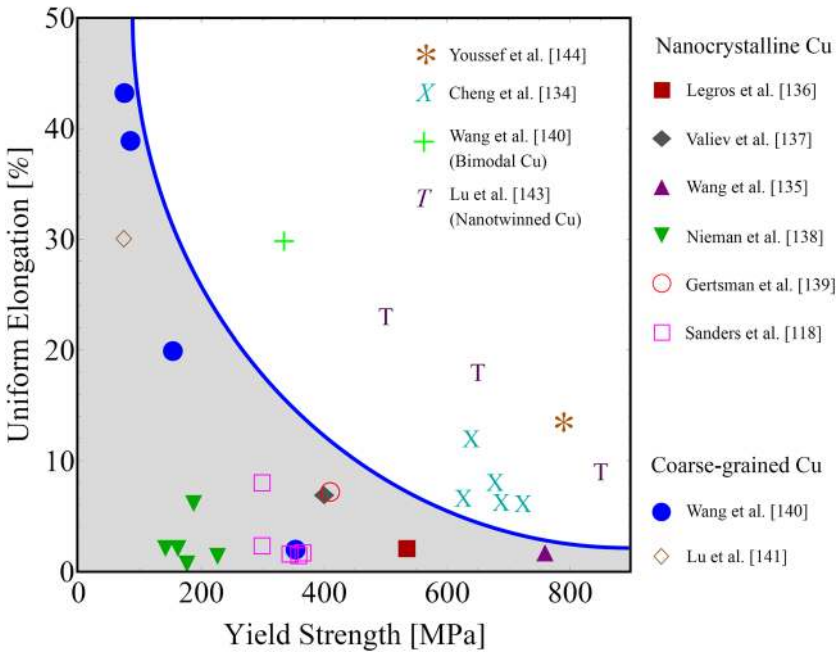

Fig. 9. The uniform elongation plotted against the *tensile* yield strength for nanocrystalline copper, as obtained from several studies. The line is used to demarcate the ductility versus strength trade-off for most nanocrystalline Cu studies in the literature[121,135–139] (versus coarse-grain copper[140,141]). However, several studies used microstructure design and consolidation to push the strength and ductility beyond this limit[134,140,143,144]

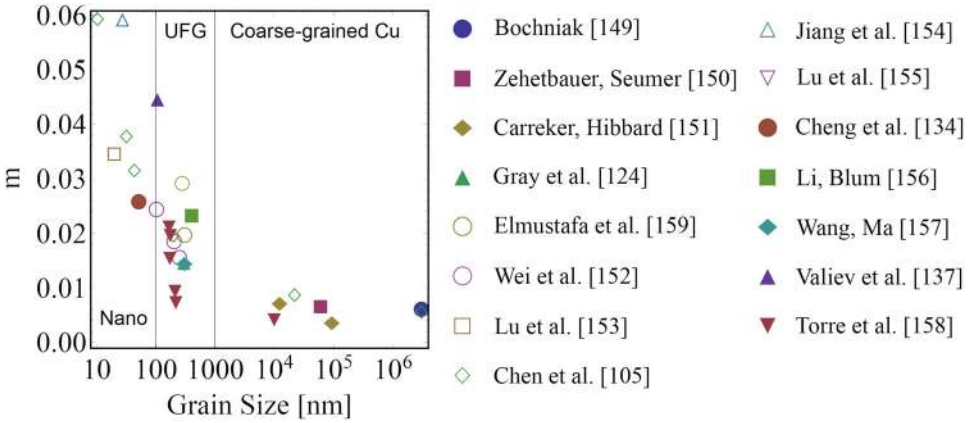

Fig. 10. The strain-rate sensitivity m increases with decreasing grain size for copper processed by a number of different methods. The different grain sizes are categorized into nanocrystalline (<100 nm), ultrafine grained (100 nm to 1μm), and coarse grained (>1 μm) for various studies[108,126,134,137,149–159]

Despite the ability to push the strength and ductility, these nanocrystalline and highly twinned microstructures still have problems with either thermal stability and/or scalability to bulk dimensions due to the processing method used.

Strain Hardening

Nanocrystalline materials typically exhibit little if any tensile elongation. This arises from the inability of nanocrystalline materials to generate and store dislocations. In general, below certain grain sizes the majority, if not all, dislocation generation and storage takes place in the grain boundary as opposed to the larger grain interior. Hence, there have been a number of studies in face-centered cubic (fcc) metals investigating the grain size associated with this behavior, the role of grain boundaries and stacking fault energy in nucleating dislocations and the subsequent behavior of dislocations afterward.[145–148] What is generally observed with the grain boundary dislocation activity is that the dislocation density increases, which results in both dynamic recovery and increased dislocation annihilation; this ultimately limits the capacity for dislocation storage.[4] This low saturation of dislocation density leads to the very low strain-hardening rate typically seen. Materials that exhibit low or zero strain hardening, such as amorphous materials, fail after yielding during tensile loading. Thus, strain hardening delays necking during tensile loading. Recent improvements in the consolidation process have increased the strain-hardening capability of nanocrystalline materials. Moreover, recent research into the use of dispersed second phases and twin boundaries enable additional sinks for trapping and storing dislocations.

Strain-Rate Sensitivity (and Activation Volume)

The strain-rate sensitivity does not consistently trend with grain size for all nanocrystalline crystal structures. For instance, in body-centered cubic (bcc) metals, the strain-rate sensitivity will generally decrease with decreasing grain size. For example, the strain-rate sensitivity coefficient m in Fe increases from 0.006 to 0.080 as the grain size increases from 20 nm to 20 μm, respectively. In contrast, however, the activation volume remains approximately constant ($\sim$10 b^3), which suggests that there is not a change in the deformation mechanism. The reduced m values for bcc metals often leads to a plastic instability, such as shear localization. On the other hand, in fcc metals, such as Cu, Al, Ni, and Au, the strain-rate sensitivity will generally increase with decreasing grain size, in contrast to bcc metals. For example, Fig. 10 shows the strain-rate sensitivity m as a function of grain size for a range of grain sizes from nanocrystalline to coarse grained and for a number of different processing methods.[108,126,134,137,149–159] The coefficient m increases with decreasing grain size. Moreover, this plot shows that the strain-rate sensitivities are as high as 3–4 times higher for ultrafine-grained Cu than for coarse-grained Cu and are as high as 6–8 times higher for nanocrystalline materials than for coarse-grained Cu. A few of the values of strain-rate sensitivity at smaller grain sizes are above $m = 0.5$, which has been associated with grain boundary sliding.[160] The rapid increase of strain-rate sensitivity in nanocrystalline Cu may indicate a change in the plastic deformation mechanism. As the strain-rate sensitivity increases with decreasing grain size, the activation volume decreases from $\sim 1000b^3$ in the coarse-grained regime to $\sim 10b^3$ in the nanocrystalline regime (e.g., Ref. 108), signaling a change in mechanism from one where dislocations cut through forest lattice dislocations to one where grain boundaries nucleate dislocations and then serve as significant obstacles to dislocation motion. For further discussion of aspects of strain-rate sensitivity, activation volume, and deformation mechanisms, the interested reader is referred to Asaro and Suresh.[161]

Creep

Creep in nanocrystalline materials is general considered to be controlled by diffusional mechanisms due to the large surface-to-volume ratio exhibited by these materials. The two main diffusional mechanisms involved in creep of coarse-grained materials are Nabarro-Herring and Coble creep. Nabarro-Herring creep involves diffusion of vacancies through the lattice and Coble creep involves diffusion along the grain boundaries. In general, creep data for nanocrystalline materials are inconsistent or not comparable due to the lack of scope in the experimental studies. As previously mentioned, the reasons for this are the structural defects related to processing of the materials including porosity, insufficient particle bonding, and contamination. These vary from report to report based on the type of processing. Second, the high density of grain boundaries and triple junctions often results in complicated creep mechanisms, for which current models are lacking. Third, grain growth of nanocrystalline materials has typically occurred at much lower temperatures than for coarse-grained materials; hence, creep studies are often limited to very low temperature ranges and/or high stress values. Last, it is difficult to produce the large bulk samples that are required for conventional creep studies. While there are a number of challenges, there are some efforts exploring creep in nanocrystalline materials that do exist,[162] in many cases investigating mechanisms such as stress-assisted grain growth.[162] Again, the ability to synthesize artifact-free bulk nanocrystalline specimens can greatly improve our ability to characterize the creep behavior of nanocrystalline materials.

Fatigue

Fatigue testing in tension has led to some interesting observations. The fatigue response in a variety of ultrafine and nanocrystalline materials has regularly shown improved endurance limits and increased crack growth rates. Fatigue response is influenced by both the frequency of fatigue oscillations and the grain boundary disorder. For instance, nanocrystalline materials generally perform better in high-cycle fatigue and perform worse in low-cycle fatigue than coarse-grained materials. Studies have shown that providing a short annealing treatment to allow for grain boundary relaxation has increased fatigue life in both regimes (high/low). There is a lot of scatter in the data related to problems with consolidation of bulk samples; the same problems are evident with other properties that require bulk specimens, such as impact toughness and crack growth studies. However, the recent ability to fully consolidate bulk nanocrystalline specimens may allow for more complete and precise studies of these sorts of properties.

Physical Properties

Electrical and Thermal Conductivity

There has been some amount of work investigating nanocrystalline copper as a high-strength material for applications that also require a high electrical conductivity. Unfortunately, because grain boundaries scatter the conducting electrons in metals, increasing the density of grain boundaries in nanocrystalline materials greatly increases the electrical resistivity (which has been reported to be larger than coarse-grained Cu[5]). However, in the case of electrodeposited nanotwinned Cu,[5] the room-temperature electrical conductivity was found to be ~97% that of the international annealed copper standard (IACS), which is only 5% less than oxygen-free high-conductivity (OFHC) Cu. More recent studies have even shown that reducing the grain boundary fraction through epitaxial synthesis (similar to single crystal), but retaining the high density of twins (for strength), results in an even better electrical conductivity than columnar nanotwinned Cu samples.[163]

Very little work has been done on the thermal conductivity of bulk nanocrystalline metals. Most of the available data are on thin layers and/or films. Recently, data have been published using scanning thermal microscopy (SThM) to map the thermal conductivity in ultrafine-grained Cu,[164,165] Fe,[166,167] and Ti[165] surface layers produced by surface mechanical attrition treatment (SMAT). In general, the ultrafine/nanograined microstructures (~100 nm) lead to a decrease in thermal conductivity. Coarse-grained microstructures of Cu, Fe, and Ti have values of 349.6 W/mK, 76.0 W/mK, and 24.6 W/mK, respectively, while the ultrafine/nanograined structures have thermal conductivities of 46.8 W/mK, 14.2 W/mK, and 5.2 W/mK for Cu, Fe, and Ti, respectively (approximately an 80% decrease in thermal conductivity due in part to grain boundary scattering[168]). It has been reported routinely that nanocrystalline metals have lower Debye temperatures.

Corrosion/Oxidation Resistance

Initially, it was not obvious that nanocrystalline materials may have an advantage when it comes to increased corrosion/oxidation resistance. The large percent microstructure constituted by grain boundaries suggests more area for chemical attack to occur. Indeed, there are numerous reports of nanocrystalline materials exhibiting increased corrosion over conventional grained materials (i.e., having worse corrosion resistance). However, in alloys capable of generating a passivation layer, the high density of grain boundaries may in fact be beneficial. The activation energy for diffusion along grain boundaries may be as much as ~50% of the activation energy for diffusion through the lattice. Therefore, the large surface-to-volume ratio of

nanocrystalline microstructures allows for rapid development of the passivating layer, resulting in dramatic improvements over coarse-grained materials. It has been reported an order of magnitude increase in oxidation resistance for nanocrystalline Fe-Cr alloys as compared to conventional coarse-grained materials of a similar composition. However, data on the corrosion resistance of nanocrystalline materials are still limited and depend both on the material as well as on the passivation layer formed. There are studies where corrosion resistance is improved, not affected, or decreased, depending mostly on the environment[169] (some of which are detailed in a recent review by Andrievski[24]). In truth, corrosion/oxidation resistance is highly dependent on material system as well as the operating mechanism for this resistance; more data may be required to determine more general trends in corrosion/oxidation.

Radiation Resistance

A substantial amount of work has investigated the radiation resistance of copper at grain sizes ranging from the coarse-grained regime to the nanocrystalline regime. As molecular dynamics simulations show that grain boundaries can act as a sink for radiation-induced point defects produced from radiation damage,[170–172] the increased density of interfaces in nanocrystalline materials results in enhanced radiation resistance. In truth, this high surface area of interfaces has similarly motivated efforts in Cu-Nb multilayered thin films for radiation resistance.[173,174] Moreover, the atomic structure of the grain boundary has been shown to have an effect on the interaction with point defects.[171,175,176] This fact suggests that increasing the concentration of certain types of boundaries may also be beneficial in radiation resistance of nanocrystalline materials. For instance, molecular dynamics simulations in Cu have shown that the Σ3 coherent twin boundary, abundant in electrodeposited nanotwinned copper, has a much smaller interaction with radiation defects than most other general boundaries.[177] In general, the density of boundaries directly affects the ability of nanocrystalline materials to absorb radiation-induced defects, but this same high density of boundaries also raises concerns about long-term radiation/thermal stability and radiation-induced segregation of deleterious elements for these applications.

Understanding Mechanisms Through Modeling and Simulations at the Atomic Scale

Various modeling and simulation techniques exist to span both the inherent length scales and time scales to understand complex mechanical and physical behavior in different material classes. For nanocrystalline materials, many interesting mechanisms for deformation and physical properties revolve around the atomic-level makeup of the grain boundary (and triple junction) structure and their interactions with surrounding grains, elements/impurities, and nanoscale precipitates. Indeed, much of the recent scientific interest in nanocrystalline materials is associated with understanding and *quantifying* the atomic-level mechanisms of plastic deformation in the grain boundaries. Some of the following discussion briefly describes findings and techniques in molecular dynamics (MD) simulations for the analysis of nanocrystalline structures. These are separated into nanocrystalline copper MD simulations, bicrystalline copper MD simulations, and recent algorithm development for analysis of MD simulations.

Nanocrystalline MD Simulations

Much of the research in nanocrystalline fcc metals has focused on ascertaining the effects of grain size, grain boundary character, and crystallographic orientation on the mechanical properties and deformation mechanisms. As previously described, nanocrystalline materials undergo a transition in deformation mechanisms from grain rotation and grain boundary sliding (smaller grain sizes) to dislocation nucleation and propagation (intermediate grain sizes) to dislocation motion and pileup (larger grain sizes), the transition of which is dependent on both strain rate and temperature.[178] MD simulations have served as an effective tool for analyzing dislocation nucleation mechanisms and GB sliding processes in nc fcc materials.[8,9,145–148] MD simulations have been used to investigate the critical grain size for transition between dislocation emission-mediated and GB-mediated deformation modes, which also corresponds to the peak strength in fcc materials[9] and the breakdown of the classic Hall–Petch relation.[8] Below this critical grain size, MD simulations have shown that GB sliding becomes the dominant deformation mechanism,[179] giving rise to grain rotation, in agreement with some experimental observations.[180] Furthermore, Van Swygenhoven and Derlet[181] have shown that GB sliding is triggered by atomic shuffling and stress-assisted free volume migration from triple junctions; the emission of dislocations from GBs was limited. In addition, three-dimensional nanocrystalline materials that undergo grain rotation have also displayed the inverse Hall–Petch response.[8,179] Above this critical grain size, MD simulations have shown that partial or full dislocation nucleation from GBs is accompanied by atomic shuffling in the GB.[182,183] Dislocation pileups at the GB in nc Cu are predicted to form in grain sizes above 50 nm.[184] As a complement to highly twinned electrodeposited structures, more recent studies have focused on the mechanical behavior and stability of nanocrystalline structures with a high density of twins,[185–189] whereby the twins provide obstacles to dislocation motion as well as dislocation nucleation sites within

the nanocrystalline grain structure. The deformation mechanisms observed in these MD simulations qualitatively agree with limited experimental results.

Grain Boundary (Bicrystal) MD Simulations

Several studies have investigated bicrystal simulation cells in an effort to determine the influence of grain boundary degrees of freedom on grain boundary properties. With this technique, the two adjoining crystal orientations, the grain boundary plane, the grain boundary structure, and the simulation cell are all controlled such that properties can be compared between different grain boundaries. In this manner, grain boundaries with beneficial and/or detrimental properties can be identified and the variation in properties with grain boundary structure can be ascertained. In contrast to nanocrystalline techniques, such techniques do not take into account the various heterogeneities that naturally exist in nanocrystalline structures: the different GB inclinations and asymmetries, the effects of triple junctions on GB structure and properties, the various crystallographic orientations and texture, etc. However, these same attributes complicate the analysis of how individual grain boundaries may impact deformation in nanocrystalline materials.

Several different properties have been explored using these techniques. Early work examined the grain boundary structures and energies of fcc metals in symmetric and asymmetric tilt grain boundaries.[190–192] In general, these studies have shown that the grain boundary has a minimum energy structure that is composed of combinations of structural units (i.e., grain boundary dislocations) from particular low-order coincident site lattice boundaries (low Σ boundaries, such as the Σ3 coherent twin boundary). For the interested reader, some recent works have calculated the structures and energies for symmetric/asymmetric tilt/twist/mixed character grain boundaries in Cu, Ni, and/or Al;[193–195] in particular, Olmsted et al.[193] explored 388 distinct Ni and Al boundaries to ascertain relationships with grain boundary energy and grain boundary mobility.[196] These methods have been extended from energies to calculating the properties of individual grain boundaries in an effort to understand grain boundary mechanics, such as dislocation nucleation,[115–118,197] grain boundary sliding,[198] spall strength,[199,200] fracture,[201] and GB-dislocation interactions.[202,203] In many cases, it was found that the grain boundary properties are not simply governed by the crystallographic orientations of the adjacent grains (e.g., see Ref. 119) nor the average properties of the boundary (e.g., energy, excess volume, etc.), but that the grain boundary structural units, the stress state,[204] and even the free volume within the boundary[112,113,205] plays an important role in the deformation characteristics.

Advancements in the Analysis of MD

There are a number of emerging tools and algorithms that can aid in analyzing the complex structure of nanocrystalline materials. Previous studies have used per-atom structure metrics (e.g., centrosymmetry,[206] slip vector,[207] common-neighbor analysis,[208] or Ackland analysis[209]) for distinguishing and visualizing grain boundaries, triple junctions, dislocations, twins, and point defects in static or dynamic simulations.[96,210] In addition to these structure-based metrics, there have emerged a number of continuum mechanics-motivated metrics that define different strain or stress measures based on the local environment, e.g., the Hardy stress by Zimmerman and colleagues,[97,211] deformation gradient-based metrics by Tucker et al.[212,213] and Stukowski and Arsenlis.[214] Moreover, the ability to track, visualize, and characterize dislocations can offer even further insight into deformation in nanocrystalline materials.[215] While many of these techniques have focused on per-atom metrics or visualization of line/planar defects, there are also a number of studies that have examined x-ray diffraction peak profiles in nanocrystalline materials to understand peak broadening due to grain size, temperature, deformation, and residual microstrain.[216–219] The ability to transform the atomistic details into an x-ray profile can allow for a direct comparison of atomistic results and details with experimental diffraction patterns.

CONCLUSION

This article discusses the synthesis and consolidation of bulk nanocrystalline materials via mechanical alloying, with a focus on nanocrystalline copper. One of the limiting steps for producing bulk nanocrystalline copper via mechanical alloying is consolidating the nanostructured powder at elevated temperatures. Hence, various approaches to thermal stability including alloying copper with solutes have been investigated. Many of the most recent approaches use the concept and analytical models of thermodynamic stability to guide efforts in producing nanocrystalline materials that are stable at high temperatures, thus enabling consolidation of the nanocrystalline material to full density in bulk form. An example of nanocrystalline Cu-Ta alloys consolidated via equal-channel angular extrusion is shown to have a nanocrystalline grain size (as low as 70 nm) after elevated temperature ECAE consolidation with a combination of fine Ta precipitates and larger Ta grains. This nanostructured microstructure provides hardness and quasi-static strengths for nanocrystalline Cu-10%Ta that rival nanocrystalline Ta at the same grain size. Moreover, both molecular dynamics simulations and analytical models agree well with experimental microstructures and behavior of these materials. Last, a number of mechanical properties of nanocrystalline copper produced using various process-

ing methods are compiled to show the change in properties with decreasing grain size.

It is a very exciting time for nanocrystalline materials. Many of the processing and consolidation challenges that have haunted nanocrystalline materials are now more fully understood, enabling bulk materials and parts to be produced. While there are still challenges remaining, recent advances in experimental, computational, and theoretical capability have now allowed for future studies with bulk specimens that have heretofore been pursued only on a limited basis. This integration of experiments and computational materials science can allow researchers to intelligently probe the compositional and processing design space for nanocrystalline materials to bring about the next generation of advanced multifunctional materials with both ultrahigh strength and good ductility for defense and energy applications.

REFERENCES

1. H. Gleiter, *Prog. Mater Sci.* 33, 223 (1989).
2. R. Valiev, *Nat. Mater.* 3, 511 (2004).
3. K.S. Kumar, H. Van Swygenhoven, and S. Suresh, *Acta Mater.* 51, 5743 (2003).
4. M.A. Meyers, A. Mishra, and D.J. Benson, *Prog. Mater Sci.* 51, 427 (2006).
5. L. Lu, Y.F. Shen, X.H. Chen, L.H. Qian, and K. Lu, *Science* 304, 422 (2004).
6. E.O. Hall, *Phys. Soc. Lond. B* 64, 747 (1951).
7. N.J. Petch, *J. Iron Steel Inst.* 174, 25 (1953).
8. J. Schiotz, F.D. Di Tolla, and K.W. Jacobsen, *Nature* 391, 561 (1998).
9. J. Schiotz and K.W. Jacobsen, *Science* 301, 1357 (2003).
10. G.J. Fan, H. Choo, K. Liaw, and E.J. Lavernia, *Mater. Sci. Eng. A* 409, 243 (2005).
11. B.Q. Han, E.J. Lavernia, and F.A. Mohamed, *Rev. Adv. Mater. Sci.* 9, 1 (2005).
12. C.C. Koch, *Scripta Mater.* 49, 657 (2003).
13. J.R. Weertman, *Mater. Sci. Eng. A* 166, 161 (1993).
14. S. Brandstetter, K. Zhang, A. Escuadro, J.R. Weertman, and H. Van Swygenhoven, *Scripta Mater.* 58, 61 (2008).
15. V.Y. Gertsman, R.Z. Valiev, N.A. Akhmadeev, and O.V. Mishin, *Mater. Sci. Forum* 225, 739 (1996).
16. R. Mitra, T. Ungar, T. Morita, G. Sanders, and J.R. Weertman, *Adv. Mater. for the 21st Century: The 1999 Julia R Weertman Symposium*, ed. Y.W. Chung, D.C. Dunand, K. Liaw, and G.B. Olson (Warrendale, PA: TMS, 1999), pp. 553–564.
17. S.W. Du and R.V. Ramanujan, *J. Non-Cryst. Solids* 351, 3105 (2005).
18. J.C. Foley and J.H. Perepezko, *Mater. Sci. Forum* 225, 323 (1996).
19. R.Z. Valiev, *J. Mater. Sci.* 42, 1483 (2007).
20. R.Z. Valiev, R.K. Islamgaliev, and I.V. Alexandrov, *Prog. Mater. Sci.* 45, 103 (2000).
21. H. Natter and R. Hempelmann, *J. Phys. Chem.* 100, 19525 (1996).
22. L. Lu, M.L. Sui, and K. Lu, *Adv. Eng. Mater.* 3, 663 (2001).
23. T. Mukai, S. Suresh, K. Kita, H. Sasaki, N. Kobayashi, K. Higashi, and A. Inoue, *Acta Mater.* 51, 4197 (2003).
24. R.A. Andrievski, *J. Mater. Sci.* 49, 1449 (2014).
25. C.C. Koch, *Nanostruct. Mater.* 9, 13 (1997).
26. C.C. Koch, K.M. Youssef, R.O. Scattergood, and K.L. Murty, *Adv. Eng. Mater.* 7, 787 (2005).
27. E. Ma, *JOM* 58, 49 (2006).
28. K.A. Darling, A.J. Roberts, Y. Mishin, S.N. Mathaudhu, and L.J. Kecskes, *J. Alloy Compd.* 573, 142 (2013).
29. T. Frolov, K.A. Darling, L.J. Kecskes, and Y. Mishin, *Acta Mater.* 60, 2158 (2012).
30. K.A. Darling, M.A. Tschopp, R.K. Guduru, W.H. Yin, Q. Wei, and L.J. Kecskes, *Acta Mater.* (2014, accepted).
31. C. Suryanarayana, *Prog. Mater. Sci.* 46, 1 (2001).
32. J. Eckert, J.C. Holzer, C.E. Krill, and W.L. Johnson, *J. Mater. Res.* 7, 1980 (1992).
33. L. Lu, L.B. Wang, B.Z. Ding, and K. Lu, *Mater. Sci. Eng. A* 286, 125 (2000).
34. L. Lu, M.L. Sui, and K. Lu, *Acta Mater.* 49, 4127 (2001).
35. H.J. Fecht, E. Hellstern, Z. Fu, and W.L. Johnson, *Metall. Trans. A* 21, 2333 (1990).
36. H.G. Jiang, Y.T. Zhu, D.P. Butt, I.V. Alexandrov, and T.C. Lowe, *Mater. Sci. Eng. A* 290, 128 (2000).
37. Y. Zhang, N.R. Tao, and K. Lu, *Acta Mater.* 56, 2429 (2008).
38. K.B. Yin, Y.D. Xia, C.Y. Chan, W.Q. Zhang, Q.J. Wang, X.N. Zhao, A.D. Li, Z.G. Liu, M.W. Bayes, and K.W. Yee, *Scripta Mater.* 58, 65 (2008).
39. Y. Huang, A. Menovsky, and F. De Boer, *Nanostruct. Mater.* 2, 587 (1993).
40. C.C. Koch, R.O. Scattergood, K.A. Darling, and J.E. Semones, *J. Mater. Sci.* 43, 7264 (2008).
41. M. Ames, J. Markmann, R. Karos, A. Michels, A. Tschöpe, and R. Birringer, *Acta Mater.* 56, 4255 (2008).
42. V.Y. Gertsman and R. Birringer, *Scripta Metall. Mater.* 30, 577 (1994).
43. K. Pantleon and M.A.J. Somers, *J. Appl. Phys.* 100, 114319 (2006).
44. K. Pantleon and M.A.J. Somers, *Mater. Sci. Eng. A* 528, 65 (2010).
45. L. Lu, N.R. Tao, L.B. Wang, B.Z. Ding, and K. Lu, *J. Appl. Phys.* 89, 6408 (2001).
46. J.R. Trelewicz and C.A. Schuh, *Phys. Rev. B* 79, 094112 (2009).
47. J. Weissmüller, *Mater. Sci. Eng. A* 179–180, 102 (1994).
48. J. Weissmuller, *Nanostruct. Mater.* 3, 261 (1993).
49. H.A. Murdoch and C.A. Schuh, *J. Mater. Res.* 28, 2154 (2013).
50. H.A. Murdoch and C.A. Schuh, *Acta Mater.* 61, 2121 (2013).
51. T. Chookajorn, H.A. Murdoch, and C.A. Schuh, *Science* 337, 951 (2012).
52. C.C. Koch, R.O. Scattergood, K.A. Darling, and J.E. Semones, *J. Mater. Sci.* 43 (23–24), (2008).
53. K.A. Darling, B.K. VanLeeuwen, J.E. Semones, C.C. Koch, R.O. Scattergood, L.J. Kecskes, and S.N. Mathaudhu, *Mater. Sci. Eng. A* 528, 4365 (2011).
54. R. Kirchheim, *Acta Mater.* 55, 5129 (2007).
55. R. Kirchheim, *Acta Mater.* 50, 413 (2002).
56. T. Chookajorn and C.A. Schuh, *Phys. Rev. B* 89, 064102 (2014).
57. K.A. Darling, M.A. Tschopp, B.K. VanLeeuwen, M.A. Atwater, and Z.K. Liu, *Comput. Mater. Sci.* 84, 255 (2014).
58. N.X. Zhou and J. Luo, *Mater. Lett.* 115, 268 (2014).
59. M. Saber, H. Kotan, C.C. Koch, and R.O. Scattergood, *J. Appl. Phys.* 113 (6), 063515 (2013).
60. W.H. Rhodes, *J. Am. Ceram. Soc.* 64, 19 (1981).
61. R.A. Andrievski, *Int. J. Powder Metall.* 30, 59 (1994).
62. J.D. Hansen, R.P. Rusin, M.H. Teng, and D.L. Johnson, *J. Am. Ceram. Soc.* 75, 1129 (1992).
63. J.R. Groza and R.J. Dowding, *Nanostruct. Mater.* 7, 749 (1996).
64. J.R. Groza, *J. Mater. Eng. Perform.* 2, 283 (1993).
65. V.M. Segal, *Mater. Sci. Eng. A* 197, 157 (1995).
66. M., Furukawa, Z. Horita, M. Nemoto, and T.G. Langdon, *J. Mater. Sci.* 36, 2835 (2001).
67. V.M. Segal, *Mater. Sci. Eng. A* 271, 322 (1999).
68. R.Z. Valiev and T.G. Langdon, *Prog. Mater Sci.* 51, 881–981 (2006).
69. M. Haouaoui, I. Karaman, H.J. Maier, and K.T. Hartwig, *Metall. Mater. Trans. A* 35A, 2935–2949 (2004).
70. O.N. Senkov, S.V. Senkov, J.M. Scott, and D.B. Miracle, *Mater. Sci. Eng. A* 393, 12 (2005).
71. J. Robertson, J.T. Im, I. Karaman, K.T. Hartwig, and I.E. Anderson, *J. Non-Cryst. Solids* 317, 144 (2003).

72. S.N. Mathaudhu, K.T. Hartwig, and I. Karaman, *J. Non-Cryst. Solids* 353, 185 (2007).
73. C. Suryanarayana and N. Al-Aqeeli, *Prog. Mater. Sci.* 58, 383 (2013).
74. K.A. Darling, R.K. Guduru, C.L. Reynolds, V.M. Bhosle, R.N. Chan, R.O. Scattergood, C.C. Koch, J. Naravan, and M.O. Aboelfotoh, *Intermetallics* 16, 378 (2008).
75. H.Q. Li, A. Misra, Z. Horita, C.C. Koch, N.A. Mara, P.O. Dickerson, and Y.T. Zhu, *Appl. Phys. Lett.* 95 (7), 071907 (2009).
76. H. Konrad, T. Haubold, R. Birringer, and H. Gleiter, *Nanostruct. Mater.* 7, 605 (1996).
77. M. Zhu, Z. Wu, M. Zeng, L. Ouyang, and Y. Gao, *J. Mater. Sci.* 43, 3259 (2008).
78. J. Eckert, J.C. Holzer, and W.L. Johnson, *J. Appl. Phys.* 73, 131 (1993).
79. M.A. Atwater, H. Bahmanpour, R.O. Scattergood, and C.C. Koch, *J. Mater. Sci.* 48, 220 (2013).
80. M.A. Atwater, D. Roy, K.A. Darling, B.G. Butler, R.O. Scattergood, and C.C. Koch, *Mater. Sci. Eng. A* 558, 226 (2012).
81. M.A. Atwater, S. Mula, R.O. Scattergood, and C.C. Koch, *Metall. Mater. Trans. A* 44A, 5611 (2013).
82. M.A. Atwater, R.O. Scattergood, and C.C. Koch, *Mater. Sci. Eng. A* 559, 250 (2013).
83. D. Roy, M.A. Atwater, K. Youssef, J.C. Ledford, R.O. Scattergood, and C.C. Koch, *J. Alloy. Compd.* 558, 44 (2013).
84. E. Botcharov, J. Freudenberger, and L. Schutz, *Int. J. Mater. Res.* 97, 1350 (2006).
85. C. Xianhua and M. Jianjun, *J. Mater. Eng. Perform.* 20, 481 (2011).
86. P.C. Millett, R.P. Selvam, and A. Saxena, *Acta Mater.* 55, 2329 (2007).
87. P.C. Millett, R.P. Selvam, and A. Saxena, *Acta Mater.* 54, 297 (2006).
88. C. Millett, R.P. Selvam, S. Bansal, and A. Saxena, *Acta Mater.* 53, 3671 (2005).
89. N.Q. Vo, J. Schafer, R.S. Averback, K. Albe, Y. Ashkenazy, and P. Bellon, *Scripta Mater.* 65, 660 (2011).
90. S. Özerinç, K. Tai, N.Q. Vo, P. Bellon, R.S. Averback, and W.P. King, *Scripta Mater.* 67, 720 (2012).
91. J. Schafer, Y. Ashkenazy, K. Albe, and R.S. Averback, *Mater. Sci. Eng. A* 546, 307 (2012).
92. P.C. Millett, R.P. Selvam, and A. Saxena, *Mater. Sci. Eng. A* 431, 92 (2006).
93. M.R. Sorensen and A.F. Voter, *J. Chem. Phys.* 112, 9599 (2000).
94. E.B. Tadmor, M. Ortiz, and R. Phillips, *Philos. Mag. A* 73, 1529 (1996).
95. L.E. Shilkrot, R.E. Miller, and W.A. Curtin, *J. Mech. Phys. Solids* 52, 755 (2004).
96. A. Stukowski, *Modell. Simul. Mater. Sci. Eng*. 18 (1), 015012 (2010).
97. J.A. Zimmerman, E.B. Webb, J.J. Hoyt, R.E. Jones, P.A. Klein, and D.J. Bammann, *Modell. Simul. Mater. Sci. Eng.* 12, S319 (2004).
98. G.J. Tucker, S. Tiwari, J.A. Zimmerman, and D.L. McDowell, *J. Mech. Phys. Solids* 60, 015012 (2012).
99. C.D. Barrett, M.A. Tschopp, and H. El Kadiri, *Scripta Mater.* 67, 309 (2012).
100. S.P. Coleman, D.E. Spearot, and L. Capolungo, *Modell. Simul. Mater. Sci. Eng*. 21 (2013).
101. J.R. Trelewicz and C.A. Schuh, *Phys. Rev. B* 79 (9), 094112 (2009).
102. Q. Wei, Z.L. Pan, X.L. Wu, B.E. Schuster, L.J. Kecskes, and R.Z. Valiev, *Acta Mater.* 59, 055020 (2011).
103. Q. Wei, B.E. Schuster, S.N. Mathaudhu, K.T. Hartwig, L.J. Kecskes, R.J. Dowding, and K.T. Ramesh, *Mater. Sci. Eng. A* 493, 58 (2008).
104. R.K. Guduru, K.A. Darling, R. Kishore, R.O. Scattergood, C.C. Koch, and K.L. Murty, *Mater. Sci. Eng. A* 395, 307 (2005).
105. R.K. Guduru, A.V. Nagasekhar, R.O. Scattergood, C.C. Koch, and K.L. Murty, *Metall. Mater. Trans. A* 37A, 1477 (2006).
106. R.K. Guduru, K.L. Murty, K.M. Youssef, R.O. Scattergood, and C.C. Koch, *Mater. Sci. Eng. A* 463, 14 (2007).
107. R.K. Guduru, K.A. Darling, R.O. Scattergood, C.C. Koch, and K.L. Murty, *J. Mater. Sci.* 42, 5581 (2007).
108. J. Chen, L. Lu, and K. Lu, *Scripta Mater.* 54, 1913 (2006).
109. M.D. Uchic, D.M. Dimiduk, J.N. Florando, and W.D. Nix, *Science* 305, 986 (2004).
110. M.D. Uchic, P.A. Shade, and D.M. Dimiduk, *Ann. Rev. Mater. Res.* 39, 361 (2009).
111. T.D. Shen, J.Z. Zhang, and Y.S. Zhao, *Acta Mater.* 56, 3663 (2008).
112. G.J. Tucker and D.L. McDowell, *Int. J. Plast.* 27, 841 (2011).
113. G.J. Tucker, M.A. Tschopp, and D.L. McDowell, *Acta Mater.* 58, 6464 (2010).
114. C.C. Koch, *J. Mater. Sci.* 42, 1403 (2007).
115. D.E. Spearot, K.I. Jacob, and D.L. McDowell, *Int. J. Plast.* 23, 143 (2007).
116. D.E. Spearot, M.A. Tschopp, K.I. Jacob, and D.L. McDowell, *Acta Mater.* 55, 705 (2007).
117. M.A. Tschopp and D.L. McDowell, *Int. J. Plast.* 24, 191 (2008).
118. M.A. Tschopp and D.L. McDowell, *Scripta Mater.* 58, 299 (2008).
119. K.M. Youssef, R.O. Scattergood, K.L. Murty, J.A. Horton, and C.C. Koch, *Appl. Phys. Lett*. 87 (2005).
120. A.H. Chokshi, A. Rosen, J. Karch, and H. Gleiter, *Scripta Metall.* 23, 1679 (1989).
121. G. Sanders, J.A. Eastman, and J.R. Weertman, *Acta Mater.* 45, 4019 (1997).
122. K.M. Youssef, R.O. Scattergood, K.L. Murty, and C.C. Koch, *Appl. Phys. Lett.* 85, 929 (2004).
123. R. Suryanarayanan Iyer, C.A. Frey, S.M.L. Sastry, B.E. Waller, and W.E. Buhro, *Mater. Sci. Eng. A* 264, 210 (1999).
124. G.E. Fougere, J.R. Weertman, R.W. Siegel, and S. Kim, *Scripta Metall. Mater.* 26, 1879 (1992).
125. S.R. Agnew, B.R. Elliott, C.J. Youngdahl, K.J. Hemker, and J.R. Weertman, *Mater. Sci. Eng. A* 285, 391 (2000).
126. G.T. Gray, T.C. Lowe, C.M. Cady, R.Z. Valiev, and I.V. Aleksandrov, *Nanostruct. Mater.* 9, 477 (1997).
127. R.Z. Valiev, E.V. Kozlov, Y.F. Ivanov, J. Lian, A.A. Nazarov, and B. Baudelet, *Acta Metall. Mater.* 42, 2467 (1994).
128. M. Haouaoui, I. Karaman, K.T. Harwig, and H.J. Maier, *Metall. Mater. Trans. A* 35, 2935 (2004).
129. E. Ma, *Scripta Mater.* 49, 663 (2003).
130. F. Ebrahimi, Q. Zhai, and D. Kong, *Scripta Mater.* 39, 315 (1998).
131. K. Hayashi and H. Eto, *J. Jpn. Inst. Met.* 53, 221 (1989).
132. M.A. Meyers and K.K. Chawla, *Mechanical Behavior of Materials* (Cambridge, U.K.: Cambridge University Press, 2009).
133. Y.H. Zhao, Y.T. Zhu, and E.J. Lavernia, *Adv. Eng. Mater.* 12, 769 (2010).
134. S. Cheng, E. Ma, Y.M. Wang, L.J. Kecskes, K.M. Youssef, C.C. Koch, U.P. Trociewitz, and K. Han, *Acta Mater.* 53, 1521 (2005).
135. Y.M. Wang, K. Wang, D. Pan, K. Lu, K.J. Hemker, and E. Ma, *Scripta Mater.* 48, 1581 (2003).
136. M. Legros, B.R. Elliott, M.N. Rittner, J.R. Weertman, and K.J. Hemker, *Philos. Mag. A* 80, 1017 (2000).
137. R.Z. Valiev, I.V. Alexandrov, Y.T. Zhu, and T.C. Lowe, *J. Mater. Res.* 17, 5 (2002).
138. G.W. Nieman, J.R. Weertman, and R.W. Siegel, *Nanostruct. Mater.* 1, 185 (1992).
139. V.Y. Gertsman, R.Z. Valiev, N.A. Akhmadeev, and O.V. Mishin, *Mater. Sci. Forum* 225–227, 739 (1996).
140. Y.M. Wang, M.W. Chen, F.H. Zhou, and E. Ma, *Nature* 419, 912 (2002).
141. L. Lu, L.B. Wang, B.Z. Ding, and K. Lu, *J. Mater. Res.* 15, 270 (2000).
142. Y.M. Wang, E. Ma, and M.W. Chen, *Appl. Phys. Lett.* 80, 2395 (2002).
143. L. Lu, X. Chen, X. Huang, and K. Lu, *Science* 323, 607 (2009).

144. K. Youssef, M. Sakaliyska, H. Bahmanpour, R. Scattergood, and C. Koch, *Acta Mater.* 59, 5758 (2011).
145. H. Van Swygenhoven, P.M. Derlet, and A.G. Froseth, *Nat. Mater.* 3, 399 (2004).
146. H. Van Swygenhoven and J.R. Weertman, *Mater. Today* 9, 24 (2006).
147. V. Yamakov, D. Wolf, S.R. Phillpot, A.K. Mukherjee, and H. Gleiter, *Nat. Mater.* 3, 43 (2004).
148. V. Yamakov, D. Wolf, S.R. Phillpot, A.K. Mukherjee, and H. Gleiter, *Philos. Mag. Lett.* 83, 385 (2003).
149. W. Bochniak, *Acta Metall. Mater.* 43, 225 (1995).
150. M. Zehetbauer and V. Seumer, *Acta Metall. Mater.* 41, 577 (1993).
151. R.P. Carreker and W.R. Hibbard, *Acta Metall.* 1, 656 (1953).
152. Q. Wei, S. Cheng, K.T. Ramesh, and E. Ma, *Mater. Sci. Eng. A* 381, 71 (2004).
153. L. Lu, S.X. Li, and K. Lu, *Scripta Mater.* 45, 1163 (2001).
154. Z.H. Jiang, X.L. Liu, G.Y. Li, Q. Jiang, and J.S. Lian, *Appl. Phys. Lett.* 88 (14), 143115 (2006).
155. L. Lu, R. Schwaiger, Z.W. Shan, M. Dao, K. Lu, and S. Suresh, *Acta Mater.* 53, 2169 (2005).
156. Y.J. Li and W. Blum, *Phys. State Solidi A* 202, R119 (2005).
157. Y.M. Wang and E. Ma, *Appl. Phys. Lett.* 83, 3165 (2003).
158. F.H.D. Torre, E.V. Pereloma, and C.H.J. Davies, *Acta Mater.* 54, 1135 (2006).
159. A.A. Elmustafa, J. Lou, O. Adewoye, W.O. Soboyejo, and D.S. Stone, *MRS Online Proceedings Library*, 750, 143115 (2002).
160. H. Luthy, R.A. White, and O.D. Sherby, *Mater. Sci. Eng.* 39, 211 (1979).
161. R.J. Asaro and S. Suresh, *Acta Mater.* 53, 3369 (2005).
162. S. Gollapudi, K.V. Rajulapati, I. Charit, C.C. Koch, R.O. Scattergood, and K.L. Murty, *Mater. Sci. Eng. A* 527, 5773 (2010).
163. O. Anderoglu, A. Misra, H. Wang, F. Ronning, M.F. Hundley, and X. Zhang, *Appl. Phys. Lett.* 93 (8), 083108 (2008).
164. F.A. Guo, Y.L. Ji, N. Trannoy, and J. Lu, *Mater. Sci. Eng. B* 130, 24 (2006).
165. F.A. Guo, Y.L. Ji, Y.N. Zhang, and N. Trannoy, *Mater. Char.* 58, 658 (2007).
166. F.A. Guo, N. Trannoy, and J. Lu, *Superlattice Microstruct.* 35, 445 (2004).
167. F.A. Guo, N. Trannoy, and J. Lu, *Mater. Chem. Phys.* 96, 59 (2006).
168. F. Bo, L. Zhixin, and Z. Xing, *J. Phys. D* 42, 083108 (2009).
169. K.D. Ralston and N. Birbilis, *Corrosion* 66 (7), 075005 (2010).
170. X.M. Bai and B.P. Uberuaga, *JOM* 65, 360 (2013).
171. X.M. Bai, A.F. Voter, R.G. Hoagland, M. Nastasi, and B.P. Uberuaga, *Science* 327, 1631 (2010).
172. I.J. Beyerlein, A. Caro, M.J. Demkowicz, N.A. Mara, A. Misra, and B.P. Uberuaga, *Mater. Today* 16, 443 (2013).
173. X. Zhang, E.G. Fu, N. Li, A. Misra, Y.Q. Wang, L. Shao, and H. Wang, *J. Eng. Mater. Technol.* 134 (4), 041010 (2012).
174. A. Misra, M.J. Demkowicz, X. Zhang, and R.G. Hoagland, *JOM* 59, 62 (2007).
175. M.A. Tschopp, M.F. Horstemeyer, F. Gao, X. Sun, and M. Khaleel, *Scripta Mater.* 64, 908 (2011).
176. M.A. Tschopp, K.N. Solanki, F. Gao, X. Sun, M.A. Khaleel, and M.F. Horstemeyer, *Phys. Rev. B* 85, 064108 (2012).
177. M.J. Demkowicz, O. Anderoglu, X.H. Zhang, and A. Misra, *J. Mater. Res.* 26, 1666 (2011).
178. H. Conrad, *Mater. Sci. Eng. A* 341, 041010 (2003).
179. J. Schiotz, T. Vegge, F.D. Di Tolla, and K.W. Jacobsen, *Phys. Rev. B* 60, 11971 (1999).
180. Z.W. Shan, E.A. Stach, J.M.K. Wiezorek, J.A. Knapp, D.M. Follstaedt, and S.X. Mao, *Science* 305, 654 (2004).
181. H. Van Swygenhoven and A. Derlet, *Phys. Rev. B* 64 (22), 224105 (2001).
182. H. Van Swygenhoven, M. Derlet, and A. Hasnaoui, *Phys. Rev. B* 66 (2), 024101 (2002).
183. M. Derlet, H. Van Swygenhoven, and A. Hasnaoui, *Philos. Mag.* 83, 3569 (2003).
184. J. Schiotz, *Scripta Mater.* 51, 837 (2004).
185. A.G. Froseth, M. Derlet, and H. Van Swygenhoven, *Appl. Phys. Lett.* 85, 5863 (2004).
186. A.J. Cao and Y.G. Wei, *J. Appl. Phys.* 102 (8), 083511 (2007).
187. I. Shabib and R.E. Miller, *Acta Mater.* 57, 4364 (2009).
188. X.Y. Li, Y.J. Wei, L. Lu, K. Lu, and H.J. Gao, *Nature* 464, 877 (2010).
189. A. Stukowski, K. Albe, and D. Farkas, *Phys. Rev. B* 82, 224103 (2010).
190. A.P. Sutton and V. Vitek, *Philos. Trans. Roy. Soc. Lond. A* 309, 1 (1983).
191. J.D. Rittner and D.N. Seidman, *Phys. Rev. B* 54, 6999 (1996).
192. U. Wolf, F. Ernst, T. Muschik, M.W. Finnis, and H.F. Fischmeister, *Philos. Mag. A* 66, 991 (1992).
193. D.L. Olmsted, S.M. Foiles, and E.A. Holm, *Acta Mater.* 57, 3694 (2009).
194. M.A. Tschopp and D.L. McDowell, *Philos. Mag.* 87, 3147 (2007).
195. M.A. Tschopp and D.L. McDowell, *Philos. Mag.* 87, 3871 (2007).
196. D.L. Olmsted, E.A. Holm, and S.M. Foiles, *Acta Mater.* 57, 3704 (2009).
197. L. Capolungo, D.E. Spearot, M. Cherkaoui, D.L. McDowell, J. Qu, and K.I. Jacob, *J. Mech. Phys. Solids* 55, 2300 (2007).
198. F. Sansoz and J.F. Molinari, *Acta Mater.* 53, 1931 (2005).
199. S.J. Fensin, J.P. Escobedo-Diaz, C. Brandl, E.K. Cerreta, G.T. Gray, T.C. Germann, and S.M. Valone, *Acta Mater.* 64, 113 (2014).
200. S.J. Fensin, S.M. Valone, E.K. Cerreta, and G.T. Gray, *J. Appl. Phys.* 112, 083529 (2012).
201. Y. Cheng, Z.H. Jin, Y.W. Zhang, and H. Gao, *Acta Mater.* 58, 2293 (2010).
202. Z.H. Jin, K. Gumbsch, K. Albe, E. Ma, K. Lu, H. Gleiter, and H. Hahn, *Acta Mater.* 56, 1126 (2008).
203. Z.H. Jin, Gumbsch, E. Ma, K. Albe, K. Lu, H. Hahn, and H. Gleiter, *Scripta Mater.* 54, 1163 (2006).
204. M.A. Tschopp, G.J. Tucker, and D.L. McDowell, *Comput. Mater. Sci.* 44, 351 (2008).
205. M.A. Tschopp, G.J. Tucker, and D.L. McDowell, *Acta Mater.* 55, 3959 (2007).
206. C.L. Kelchner, S.J. Plimpton, and J.C. Hamilton, *Phys. Rev. B* 58, 11085 (1998).
207. J.A. Zimmerman, C.L. Kelchner, A. Klein, J.C. Hamilton, and S.M. Foiles, *Phys. Rev. Lett.* 87, 165507 (2001).
208. H. Jonsson and H.C. Andersen, *Phys. Rev. Lett.* 60, 2295 (1988).
209. G.J. Ackland and A.P. Jones, *Phys. Rev. B* 73, 054104 (2006).
210. A. Stukowski, *Modell. Simul. Mater. Sci. Eng.* 20 (4), 045021 (2012).
211. J.A. Zimmerman, D.J. Bammann, and H.J. Gao, *Int. J. Solids Struct.* 46, 238 (2009).
212. G.J. Tucker, J.A. Zimmerman, and D.L. McDowell, *Int. J. Eng. Sci.* 49, 1424 (2011).
213. G.J. Tucker, J.A. Zimmerman, and D.L. McDowell, *Modell. Simul. Mater. Sci. Eng.* 18 (1), 015002 (2010).
214. A. Stukowski and A. Arsenlis, *Modell. Simul. Mater. Sci. Eng.* 20 (3), 035012 (2012).
215. A. Stukowski and K. Albe, *Modell. Simul. Mater. Sci. Eng.* 18, 085001 (2010).
216. S. Brandstetter, Z. Budrovic, S. Van Petegem, B. Schmitt, E. Stergar, M. Derlet, and H. Van Swygenhoven, *Appl. Phys. Lett.* 87, 231910 (2005).
217. S. Brandstetter, M. Derlet, S. Van Petegem, and H. Van Swygenhoven, *Acta Mater.* 56, 165 (2008).
218. M. Derlet, S. Van Petegem, and H. Van Swygenhoven, *Phys. Rev. B* 71 (2005).
219. A. Stukowski, J. Markmann, J. Weissmuller, and K. Albe, *Acta Mater.* 57, 1648 (2009).